Diagenesis, provenance and reservoir quality of Triassic TAGI sandstones from Ourhoud field, Berkine (Ghadames) Basin, Algeria

C. Rossi[a,*], O. Kälin[b], J. Arribas[a], A. Tortosa[a]

[a]*Departamento de Petrología y Geoquímica, Universidad Complutense de Madrid, 28040 Madrid, Spain*
[b]*Departamento de Paleontología, Universidad Complutense, 28040 Madrid, Spain*

Abstract

The Triassic TAGI (Trias Argilo-Gréseux Inférieur) fluvial sandstones are the main oil reservoirs in the Berkine Basin, Algeria. Nonetheless, their provenance and diagenesis, and their impact on reservoir quality, are virtually unknown. Samples from the Ourhoud field, representing the Lower, Middle and Upper TAGI subunits, were studied using a combination of petrographic, mineralogical and geochemical techniques. The Lower TAGI sandstones have an average framework composition of $Q_{98.3}F_{0.6}R_{1.1}$ and 95% of the quartz grains are monocrystalline. By contrast, the Middle–Upper TAGI sandstones have an average framework composition of $Q_{88.3}F_{9.8}R_{1.9}$ and 79.7% of the quartz grains are monocrystalline. The Lower TAGI quartz arenites derived from Paleozoic siliciclastic rocks, whereas the Middle–Upper TAGI subarkoses originated mainly from metamorphic terrains. This change in provenance is a potential criterion for correlation within the TAGI. Also, this change has contributed to the significantly different diagenetic paths followed by the Lower TAGI quartz arenites and the Middle–Upper TAGI subarkoses.

Grain-coating illitic clays are abundant in the Lower TAGI, where they exert a critical control on reservoir quality. These clays are interpreted as pedogenic and/or infiltrated in origin and to have had, in part, smectitic precursors. Shallow burial Fe-dolomite cementation was favored in the downthrown block of the field-bounding fault, where it contributed to the poor reservoir quality. Magnesite–siderite cements are multiphase. The earliest generation is composed of Fe-rich magnesite that precipitated during shallow burial from hypersaline fluids with high Mg/Ca ratios, probably refluxed residual brines associated with the Liassic evaporites. Later magnesite–siderite generations precipitated during deeper burial from waters with progressively higher Fe/Mg ratios. Authigenic vermicular kaolin largely consists of dickite that replaced previously formed kaolinite. Dickitization was followed by late-stage illitization related to the dissolution of detrital and authigenic K-feldspar. Quartz, the most abundant cement, was mainly sourced by the pressure- or clay-induced dissolution of detrital quartz and is a critical factor controlling the reservoir quality. Overall, quartz cement is more abundant in the Lower TAGI than in the Middle–Upper TAGI, and this increase correlates with a decrease in average porosity. Within the Lower TAGI, quartz cement abundance is stratigraphically very variable, which is in part related to facies controlled variations in grain-coating clay, resulting in major vertical variations in reservoir quality. Anhydrite and barite cements postdate quartz overgrowth. The sulfate necessary for their formation was likely sourced by deep subsurface dissolution of Late Triassic–Liassic evaporites.

Keywords: Sandstone diagenesis; Reservoir quality; Berkine basin; Triassic; Algeria

1. Introduction

Detrital composition can critically influence the reservoir quality of sandstones by conditioning the pathway of both physical and chemical diagenesis (e.g. Bloch, 1994). Intraformational variations in detrital composition can thus cause significant heterogeneity in sandstone reservoir quality. Compositional changes respond to variations in climate, depositional facies and, especially, provenance. Recognition of vertical changes in composition resulting from changes in provenance thus has great potential for improving stratigraphic resolution on a regional scale and, hence, reservoir correlation. This is especially useful in non-marine sandstones that typically lack age-diagnostic fossils (e.g. Morton & Hurst, 1995).

The fluvial sandstones of the TAGI (Trias Argilo-Gréseux Inférieur) constitute the main oil reservoirs in the Berkine Basin (Algeria). This basin hosts some of the most important recently discovered hydrocarbon accumulations in North Africa (Cochran & Petersen, 2000; MacGregor, 1998a,b). Although TAGI sandstones have relatively high porosities and permeabilities in many fields, reservoir quality varies greatly across the Basin and within individual

* Corresponding author. Tel.: +34-91-394-5014; fax: +34-91-544-2535.
E-mail address: crossi@geo.ucm.es (C. Rossi).

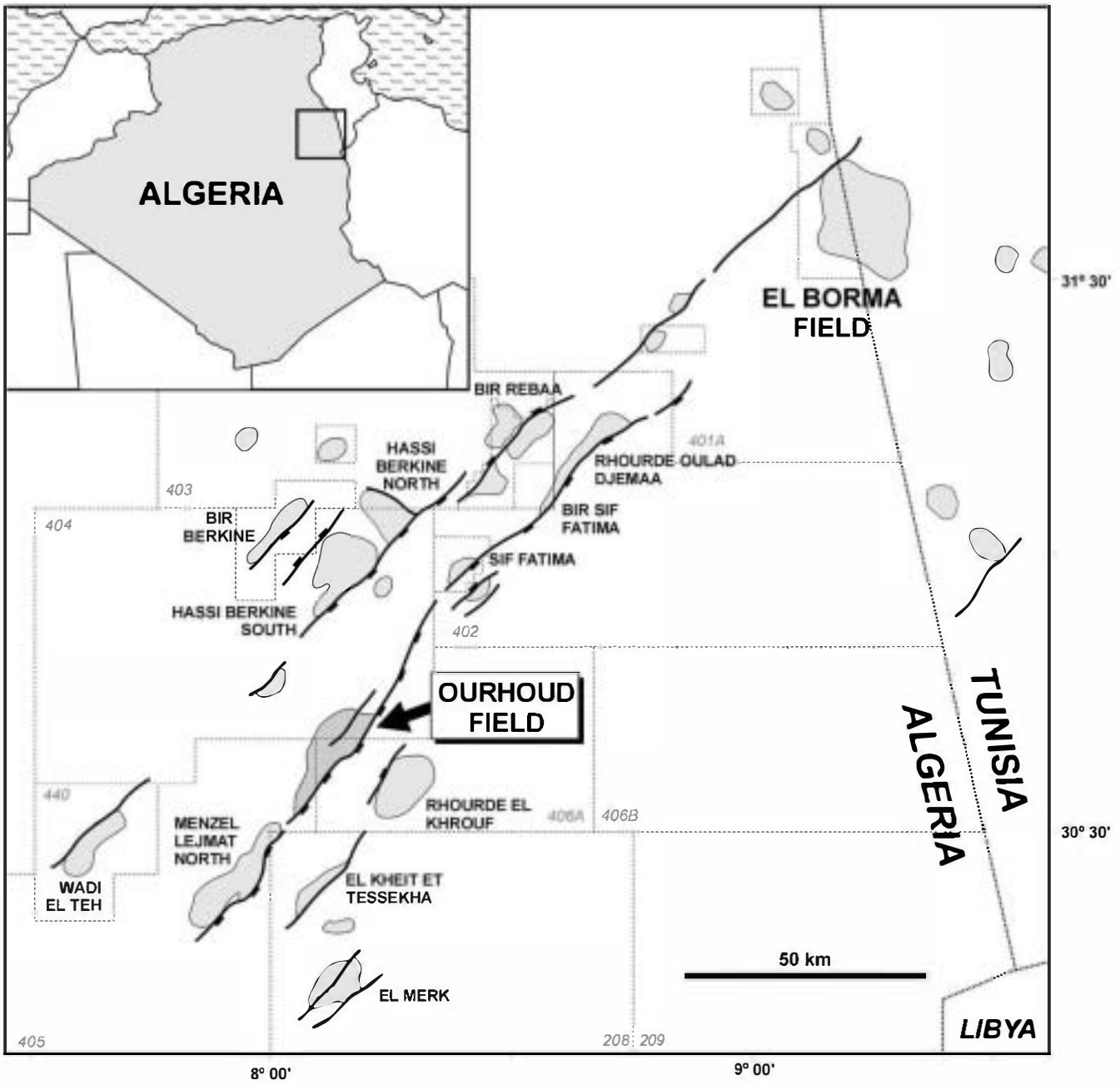

Fig. 1. Location map of the Ourhoud field in the Berkine Basin, Algeria, showing the main oil fields and faults in the area.

fields. This has been primarily attributed to the complex depositional architecture (Echikh, 1998). Therefore, considerable research effort has been made on the sedimentology and stratigraphy of these deposits (Carney et al., 1999; Scott & Wheller, 1999; Wheller et al., 1999; Turner et al., 2001). However, little is known of the provenance and diagenesis of these sandstones, and the implications of these factors for reservoir quality (Echikh, 1998). With the aim of helping to close this gap, this paper describes the compositional and diagenetic features of the TAGI sandstones in two wells from the Ourhoud field (Fig. 1) and discusses their provenance and diagenetic evolution, as well as the influence of these factors on reservoir quality. In particular, this study reveals that the TAGI succession contains a significant intraformational change in detrital composition caused by a change in provenance. This change in composition provides a potential criterion for stratigraphic correlation within the TAGI. This paper also illustrates that the reservoir quality of the TAGI sandstones is largely controlled by the distinct pathways of diagenesis followed by the sandstones of the Lower and Middle–Upper parts of the TAGI. This variation in diagenesis is mainly related to differences in initial feldspar content and in syndepositional grain-coating illitic clays.

2. Geological background

The intracratonic Ghadames Basin contains up to 6 km of Paleozoic and Mesozoic sediments and stretches over parts of eastern Algeria, western Libya and southern Tunisia (Fig. 1) (Acheche, M'Rabet, Ghariani, Ouahchi, & Montgomery, 2001). The term 'Berkine Basin' refers to the western, Algerian part of the Ghadames Basin (Cochran & Petersen, 2000). In the subsurface, the Berkine Basin is limited to the west and north by the Hassi Messaoud and Dahar structural ridges, respectively. Southward, the Berkine Basin is separated from the Illizi Basin by the Mole D'Ahara, which acted as a continental paleohigh during the Mesozoic and Cenozoic (Gauthier, Boudjema, & Lounis, 1995).

The Paleozoic (Cambrian to Early Carboniferous) fill in the Berkine Basin consists of a predominantly siliciclastic succession reaching up to 3.5 km in thickness (Askri et al., 1995) (Fig. 2). The Hercynian orogeny caused uplift and partial erosion along the basin margins. During the early Mesozoic, an extensional basin was superimposed on the pre-existing Paleozoic basin. The Mesozoic basin records sedimentation on a southern continental margin of the Tethyan sea and contains up to 4 km of sediments (Boote, Clark-Lowes, & Traut, 1998) (Fig. 3). Continental Triassic deposits were deposited over a Hercynian unconformity in a series of northeast-trending grabens that opened to the proto-Tethys toward the northeast (Boudjema, 1987; Jackson, Moore, Quarles, & Bellis, 1996). Prevalent marginal marine conditions since the Late Triassic resulted in a thick succession of Upper Triassic and Liassic evaporites, which are overlain by Late Jurassic to Early Cretaceous carbonates and siliciclastics (Askri et al., 1995) (Fig. 2).

An early Aptian phase of deformation resulted in strike-slip faulting, localized tectonic inversion and uplift (Boote et al., 1998; Echikh, 1998; Jackson et al., 1996). Renewed late Aptian to Senonian subsidence resulted in the sedimentation of a carbonate- and evaporite-dominated succession, up to 1 km thick (Fig. 3). Eocene to Miocene compressional tectonic activity caused subtle folding, uplift, and erosion, especially to the north (Boote et al., 1998). Tertiary sediments are preserved only in the central parts of the basin and consist of a relatively thin (<200 m) Miocene to Pliocene succession unconformably overlying Upper Cretaceous strata.

The Ourhoud (ORD) oil field, subject of the present study, is located within the central part of the Berkine Basin. Here, most of the oil fields discovered lie along a SW–NE oriented trend (Fig. 1). This trend contains at least six fields which have reserves exceeding 250 million barrels of oil equivalent (MMBOE), and three of them (El Borma, Hassi Berkine South, and ORD) have reserves >1000 MMBOE (Carney et al., 1999; Cochran & Petersen, 2000; MacGregor, 1998a,b; Shirley, 2000). Most of this oil is reservoired in TAGI sandstone in structural traps sealed by Liassic evaporites. The traps originated as tilted fault blocks during the Late Triassic–Liassic extension phase and some of them were later modified by the Aptian transpressive deformation (Boote et al., 1998; Cochran & Petersen, 2000; Echikh, 1998; Jackson et al., 1996).

Lower Silurian and Upper Devonian (Frasnian) black shales are the primary petroleum source rocks across the whole Saharan Platform, including the Berkine Basin (Makhous, Galushkin, & Lopatin, 1997; Yahi, Schaefer, & Littke, 2001). In the northwestern part of the basin, these source rocks subcrop the Hercynian unconformity and are thus in direct contact with Triassic sandstones (Fig. 2). This facilitated lateral updip migration to the southeast, charging Triassic sandstones in structural traps sealed by Triassic–Liassic mudstones and evaporites. The oil fields of the central part of the Berkine Basin are located a relatively short distance updip of the Devonian subcrop and thus the Frasnian shales constitute the most likely hydrocarbon sources (Fig. 2). In fact, two-dimensional basin modeling and maturity data (Yahi et al., 2001) support the hypothesis of a Frasnian source for the oils of ORD and nearby fields. According to the same authors, in the central Berkine Basin petroleum generation from the Frasnian source beds peaked during the Late Cretaceus–Tertiary, and these source rocks are currently in a mature to late mature stage.

2.1. TAGI stratigraphy

The Carnian TAGI sandstones are present over a large part of the Berkine Basin, covering the Hercynian unconformity (Fig. 2). They can exceed 100 m in thickness and pass to the NW into shales and volcanic rocks (Boudjema, 1987). In the central and SW parts of the basin, most TAGI sandstones were deposited in fluvial braidplains that drained NE (Cochran & Petersen, 2000; Wheller et al., 1999). Stratigraphically upward and toward NE, the braided-river sandstones grade into meandering river deposits, which in turn pass in the El Borma area into tide-influenced deltaic sediments (Ben Tahar, 1991; Echikh, 1998). The overall transgressive character of the TAGI culminated with the deposition of the coastal to shallow marine shales and carbonates of the 'Triassic Carbonate' unit (Boudjema, 1987).

The TAGI contains several laterally extensive mudstone intervals (Acheche et al., 2001; Boudjema, 1987), which are interpreted, in part, to be lacustrine in origin (Carney et al., 1999; Wheller et al., 1999). In the central-western part of the Berkine Basin, the presence of these intervals has allowed the subdivision of the TAGI into three main sandstone/mudstone units (i.e. Lower, Middle and Upper; Fig. 3; Ford and Scott, 1997; Cochran & Petersen, 2000; Scott & Howells, 2000). According to Daniels, Hook, Sorensen, and Emme (1994), the lower TAGI is transgressive and represents a third-order sequence. In the ORD field, the Lower TAGI can be further subdivided into three subunits referred to, in the following, as TL1, TL2, and TL3 (Fig. 3).

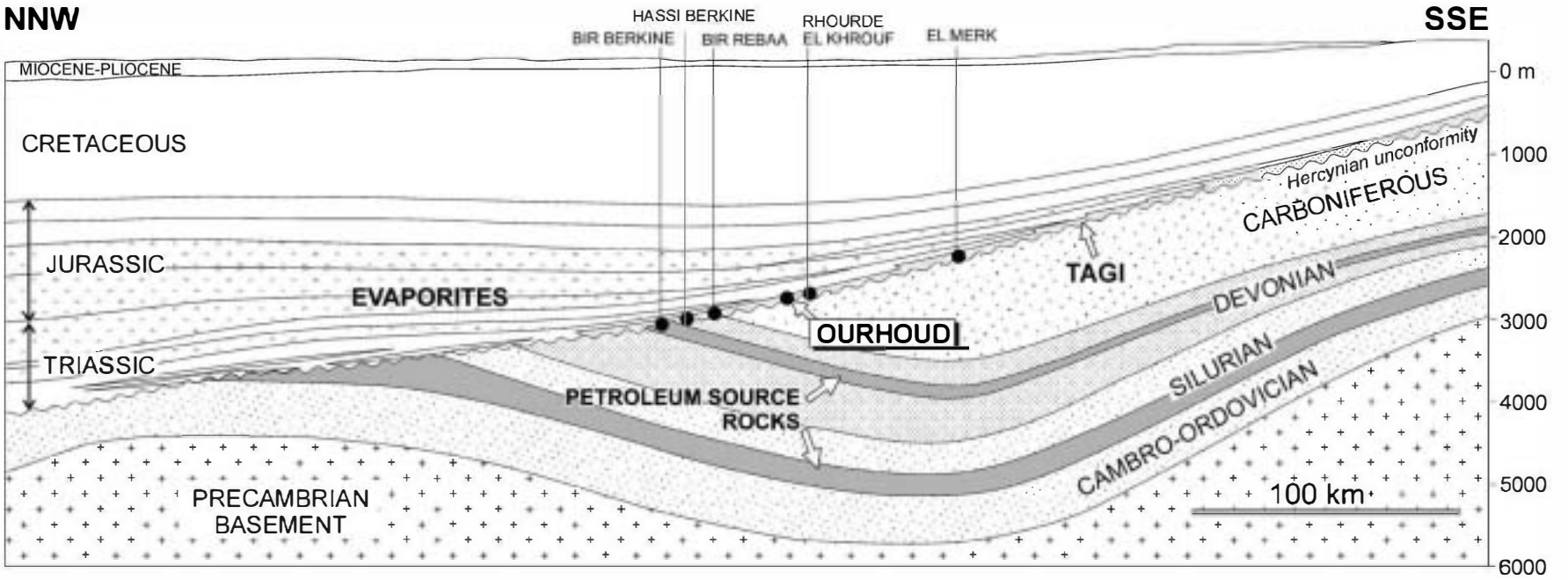

Fig. 2. NNW–SSW generalized cross section through the Berkine Basin, showing the location of major oil fields of the central part of the basin. Modified from Boote et al. (1998).

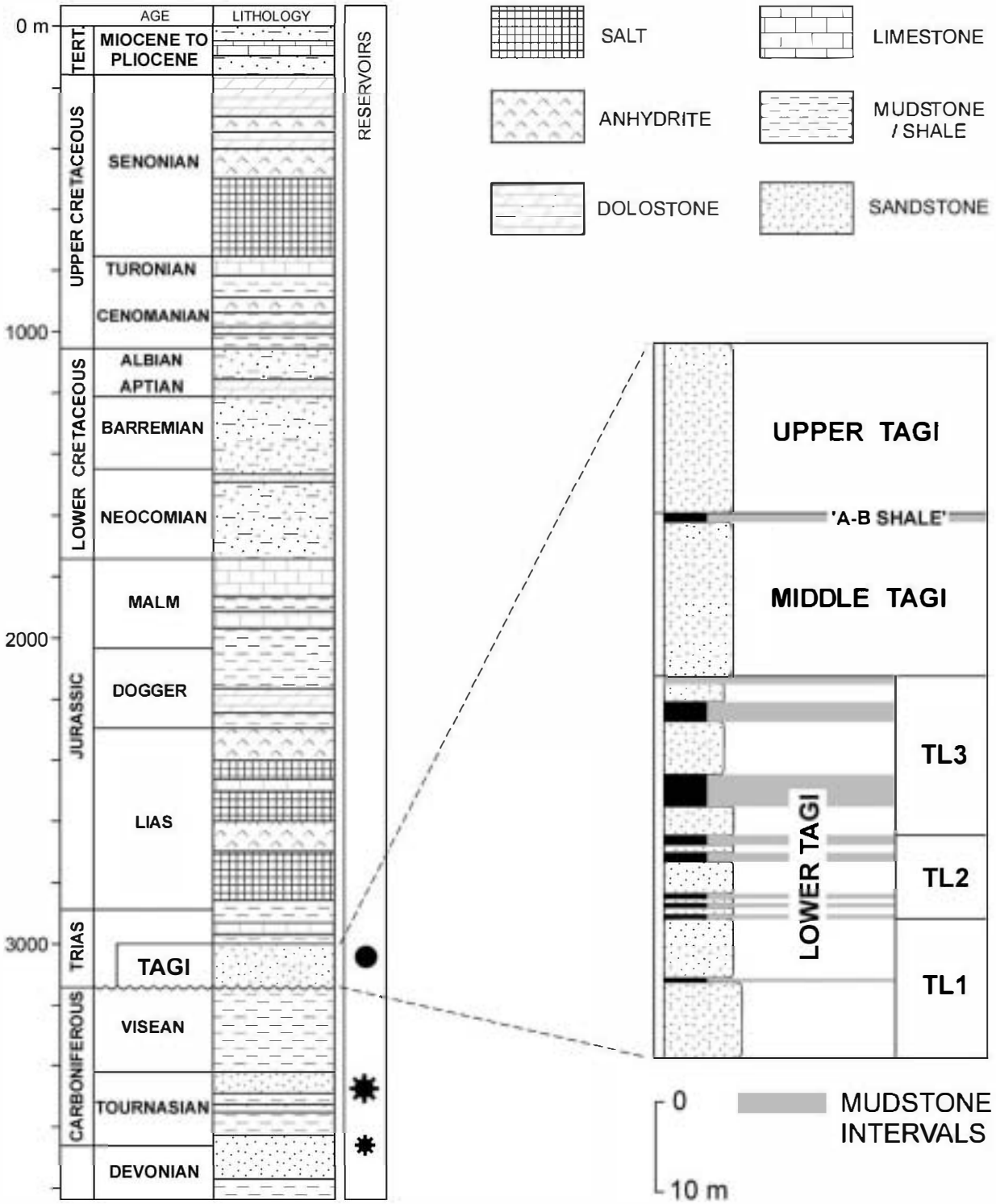

Fig. 3. Generalized stratigraphy of the Ourhoud field area, showing the location of the main hydrocarbon reservoirs and a scheme of the stratigraphic subdivision of the TAGI.

The mudstone bed that separates the Middle TAGI from the Upper TAGI, known as the 'A–B shale', is a regional stratigraphic marker. Towards the northeast, it contains marine fossils (Ben Tahar, 1991), suggesting that mudstone deposition, at least in this stratigraphic level, may be related to relative sea-level rise. Minor unconformities, locally marked by paleosols, occur at the top of the major mudstone units (Ben Tahar, 1991). This suggests that some of the sandstone–mudstone sequences may have formed in response to cyclical variations in base level, likely to be related to relative sea-level changes.

Table 1
Modal compositions of selected representative sandstones

Sample depth (m)	3306.65	3304.45	3293.5	3290.75	3271.12	3261.75	3256.75	3253.7	3249.45	3241.7	3239.67	3228.86
Unit	TL1 (%)	TL1 (%)	TL1 (%)	TL1 (%)	TL3 (%)	TL3 (%)	Middle (%)	Middle (%)	Middle (%)	Upper (%)	Upper (%)	Upper (%)
Quartz monocrystalline, undulosity < 5°	43.5	40.5	57.3	40.5	54.0	43.3	35.0	39.5	31.3	25.3	36.8	27.8
Quartz monocrystalline, undulosity >5°	17.3	17.0	9.3	22.0	14.8	12.5	14.0	9.8	18.0	14.8	14.8	9.5
Quartz polycrystalline 2–3 subgrains	1.3	2.8	3.3	4.5	3.5	2.3	6.3	4.8	5.0	5.5	6.0	4.8
Quartz polycrystalline >3 subcrystals	0.8	1.5	1.0	0.8	0.3	0.0	6.3	8.5	6.0	8.0	8.5	5.0
Carbonate replacement of quartz	0.0	0.5	0.3	0.0	0.0	1.0	0.0	0.0	2.8	5.0	0.0	0.8
Anhydrite/barite replacement of quartz	0.0	0.0	0.0	0.0	0.0	0.0	0.3	0.0	0.0	0.0	1.3	0.5
K-feldspar, single crystals	0.0	0.0	1.5	0.0	0.5	0.8	2.8	5.3	3.5	2.5	3.8	7.3
Carbonate/sulphate replacement of K-feldspar	0.0	0.0	0.0	0.0	0.0	0.5	0.0	0.0	0.5	1.5	0.0	0.5
Plagioclase, single crystals	0.0	0.0	0.0	0.0	0.0	0.0	0.0	0.0	0.3	0.3	0.0	0.3
Kaolin, replacement of feldspar	0.0	0.0	0.0	0.0	0.0	0.3	1.0	1.5	1.0	1.0	0.0	1.3
Metamorphic rock fragments	0.0	0.0	0.0	0.0	0.0	0.0	1.0	0.0	0.3	0.0	0.5	0.8
Plutonic rock fragments	0.0	0.0	0.0	0.0	0.0	0.0	0.3	0.0	0.0	0.3	0.0	0.0
Sandstone rock fragments	4.0	8.5	0.0	0.0	0.0	0.0	0.0	1.3	0.5	0.0	0.3	0.0
Mica	0.0	0.0	0.0	0.0	0.0	0.0	0.3	0.3	0.0	0.3	0.0	0.0
Stable heavy minerals (Zircon, rutile, tourm,...)	0.0	0.0	0.5	0.0	0.5	0.3	0.0	0.0	0.0	0.0	0.3	0.0
Argillaceous intraclasts	3.0	0.5	0.3	2.3	0.0	0.8	5.3	3.0	6.8	3.3	3.0	14.5
Siderite replacing argillaceous intraclasts	0.8	1.3	0.0	0.0	0.0	0.0	1.8	0.0	1.3	3.5	0.0	1.0
Pyrite replacing argillaceous intraclasts	0.0	0.0	0.0	0.0	0.0	0.0	0.8	0.0	0.3	0.3	0.0	0.5
Argillaceous laminae	0.0	0.0	0.0	0.0	0.0	0.0	0.5	0.0	0.0	0.0	0.0	8.5
Framework total	70.5	72.5	73.3	70.0	73.5	61.5	75.3	74.0	77.3	71.3	75.3	82.8
Clay coatings	1.5	1.3	13.0	14.0	11.3	4.0	0.0	0.0	0.8	0.0	0.3	0.5
K-feldspar overgrowths	0.0	0.0	0.0	0.0	0.0	0.0	0.5	0.8	0.3	0.8	0.3	1.8
Vermicular kaolin cement	0.0	0.0	3.0	0.5	1.8	2.0	1.3	1.8	0.8	0.0	0.5	0.0
Fe-dolomite cement	0.0	0.0	0.0	0.0	0.0	0.0	0.0	0.0	0.0	0.0	0.0	0.0
Quartz overgrowths	12.5	10.3	1.8	4.8	1.5	24.8	9.3	8.8	7.5	6.5	5.3	5.0
Siderite–magnesite cement	1.0	1.3	3.3	0.0	2.3	1.8	3.5	0.0	2.8	10.5	0.3	2.5
Barite cement	0.0	0.0	0.0	0.0	0.0	0.0	0.3	0.0	0.0	0.0	3.8	0.3
Anhydrite cement	0.0	0.0	0.0	0.0	0.0	0.0	0.0	0.5	0.0	0.0	1.0	0.8
Bitumen	0.0	0.0	0.0	0.0	0.0	0.0	0.0	0.0	0.0	0.0	0.0	0.0
Pyrite cement	0.0	0.0	0.0	0.0	0.0	0.0	0.3	0.0	0.0	0.5	0.0	0.0
Thin section porosity (total)	14.0	14.3	5.5	10.8	9.8	3.5	9.5	14.3	10.8	10.5	12.3	6.3
Primary porosity	11.5	11.5	4.0	9.3	8.0	1.8	7.3	10.0	7.8	8.5	7.5	4.3
Secondary porosity after feldspar	2.5	2.8	1.5	1.5	1.8	1.8	1.8	3.0	2.3	1.5	3.5	1.5
Secondary porosity after cem feldspar	0.0	0.0	0.0	0.0	0.0	0.0	0.5	1.3	0.8	0.5	1.3	0.5
Helium porosity	14.9	13.9	18.8	19.1	16.8	6.1	19.0	19.5	17.3	17.8	18.9	15.5
Permeability (Md)	960.0	341.0	12.0	12.0	8.2	0.1	1082.0	591.0	520.0	2573.0	716.0	91.0
Grain size	mL	mU-crsL	mL	mL	fU	fU	mU	fU	fU	mL	mL	fU
Sorting	ws	ws	mws	ws	ws	ews	ps	ws	ws	ws	ews	ws
Original porosity (estimated)	39.0	39.0	34.0	39.0	39.0	42.4	30.7	39.0	39.0	39.0	40.8	39.0
Intergranular volume	27.0	24.8	25.3	28.5	24.8	36.8	23.1	23.0	20.5	27.3	21.3	17.2

3. Materials and methods

Thirty selected core-plug sandstone samples were studied from a well (well A) in which reservoir quality is representative of normal field conditions (i.e. porosity and permeability values close to field average; Jorge Navarro, pers. comm.). Ten additional cutting samples were analyzed from a second well (well B, where no cores were taken), located close to the major NE-trending field-bounding fault zone. In well B, the TAGI sandstones have gamma ray values similar to well A, but log-deduced porosities are significantly lower, suggesting possible diagenetic differences between the two wells. The samples represent, in similar proportions, the Lower TAGI (21 samples, ~32 m of sandstone), and the Middle–Upper TAGI (19 samples, ~32 m of sandstone). After removing oil using acetone, plug slices were impregnated with dyed resin and ground deeply enough to remove any potential artifact porosity (cf. Pittman, 1992). Two sets of double-polished thin sections, one of them stained for K-feldspar (using sodium cobaltnitrite) and carbonates (using alizarine red-s and potassium ferricyanide), were prepared for petrographic study. Quantification of mineralogy and porosity was achieved by counting 400 points per thin section. Bulk and clay mineralogy was confirmed and determined, respectively, by X-ray diffraction (XRD). Freshly broken and polished sample surfaces were studied using a JEOL JSM 6400 scanning electron microscope (SEM) equipped with an energy dispersive X-ray (EDX) microanalyzer, in secondary electron and backscattered electron (BSE) modes. Cathodoluminescence (CL) petrography was carried out using a Technosyn MK4 luminoscope. The chemical composition of carbonate cements was determined by wavelength-dispersive X-ray spectrometry using a JEOL JXA-8900 electron microprobe (15 kV accelerating voltage, 21.5 nÅ beam current, 5 μm beam size). Detection limits were approximately 100 ppm for Mg, 150 ppm for Ca, 250 ppm for Mn and 300 ppm for Fe. The results were normalized to 100 mol% $CaCO_3$, $MgCO_3$, $FeCO_3$, $MnCO_3$, and $SrCO_3$.

4. Results

4.1. Depositional texture

The sandstones of the Lower TAGI show an overall fining-upwards trend (Table 1). In the basal part, they are typically moderately well to very well sorted and lower fine- to lower coarse-grained. Stratigraphically higher up, sandstones are typically moderately well sorted and upper fine to upper medium grained. In the uppermost portion of the Lower TAGI, sandstones are extremely well sorted and fine grained. Many Lower TAGI sandstones show lamination defined by variations in grain size. The finer-grained laminae typically contain abundant grain-coating clay and show a denser packing, as a result of enhanced chemical compaction. Intergranular clay is abundant in subunit TL2, ranging from 14 to 26 vol%. By contrast, most sandstones from subunit TL1 contain <5% of detrital or authigenic clays. Detrital quartz grains are usually very well rounded in the Lower TAGI. An exception is the clay-rich sandstones in subunit TL2, where numerous quartz grains show corrosion embayments.

In the Middle–Upper TAGI sandstones, the average grain size is upper fine sand (range: lower fine to upper medium) and most samples are well to very well sorted and lack significant detrital clay matrix (Table 1). However, detrital clay occurs as local concentrations along stylolites, which are more common in the Upper TAGI, and also along laminae defined by concentrations of argillaceous intraclasts. These argillaceous grains are usually deformed by compaction and largely converted into pseudomatrix.

4.2. Detrital composition

The sandstones of the Lower and Middle–Upper TAGI have different detrital composition.

4.2.1. Lower TAGI

The Lower TAGI sandstones are quartz arenites, with the framework consisting predominantly of monocrystalline quartz grains (Fig. 4, Table 1). The average composition is $Q_{98.3}F_{0.6}R_{1.1}$ (Fig. 4A). K-feldspar typically represents <1% of the framework. Plagioclase is absent. Detrital feldspar was partly dissolved and/or replaced by kaolin during diagenesis. Nevertheless, restored feldspar content is remarkably low: $Q(r)_{97.2}F(r)_{1.7}R(r)_{1.1}$ (Fig. 4B). Restored feldspar contents are obtained by adding to actual contents the percentages of secondary porosity formed by dissolution of feldspar grains and of authigenic minerals interpreted to have replaced feldspars. The content of sand-grade mudstone intraclasts is variable, commonly <5 vol%, but higher in laminated samples. Mudstone clasts are mainly composed of illite, which is also the predominant detrital clay in the interbedded mudstones. Mica and heavy minerals (zircon, tourmaline and rutile) appear in accessory quantities (<0.5 vol%). Sedimentary rock fragments (quartzarenitic to subarkosic sandstones) are common towards the base. The relative abundance of quartz types is $Qm_{94.7}Qp2{-}3_{4.2}Qp>3_{1.1}$, where Qm is monocrystalline quartz, Qp2–3 polycrystalline quartz with 2–3 subcrystals, and Qp > 3 polycrystalline quartz with >3 subcrystals (Fig. 4C). Under CL, the quartz grains show both red-brown and blue colors, with the occasional presence of bright red grains. A large number of quartz grains show inherited abraded overgrowths, which are more obvious in matrix-rich sandstones.

4.2.2. Middle–Upper TAGI

The Middle–Upper TAGI sandstones are subarkoses, with the framework dominated by quartz, K-feldspar and mud intraclasts (Fig. 4, Table 1). Similar to the Lower

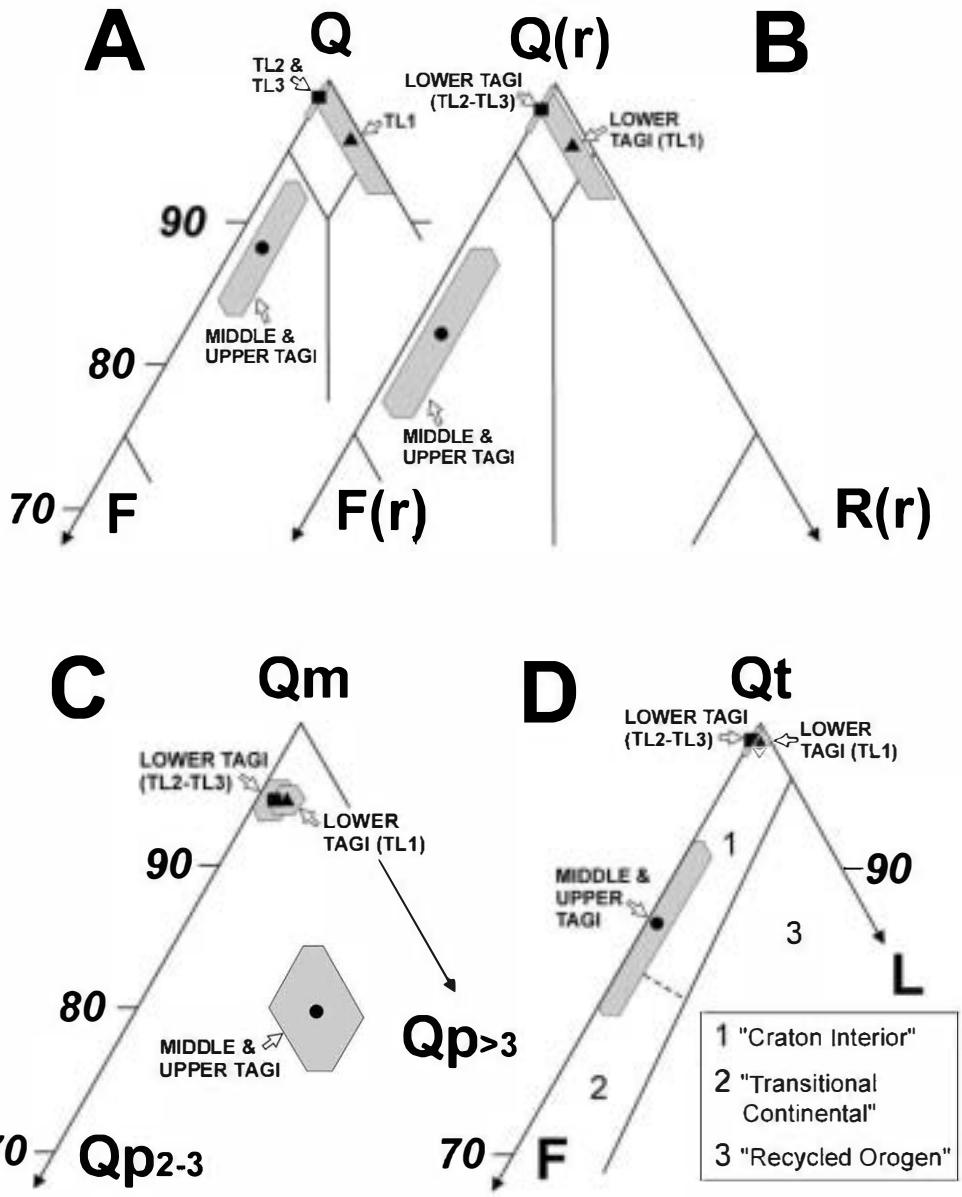

Fig. 4. Triangular plots of compositional parameters. A and B: QFR (quartz, feldspar and rock fragments) diagrams using actual (A) and restored (B) compositions. C: relative abundance of quartz types (see text for explanation). D: QtFL provenance diagram (Dickinson, 1985).

TAGI, detrital feldspar was partially eliminated during diagenesis. Actual and restored average compositions are $Q_{88.3}F_{9.8}R_{1.9}$ and $Q(r)_{82.9}F(r)_{15.4}R(r)_{1.7}$, respectively (Fig. 4A,B). Plagioclase grains (0–4.4% of the framework) are less common than K-feldspar grains. Illitic intraclasts are minor but common components, especially towards the top of the Upper TAGI. They typically occur concentrated in laminae, locally favoring stylolitization. Other minor framework components include micas, metamorphic rock fragments (quartzose–micaceous schists), granitic rock fragments, heavy minerals (zircon, tourmaline and rutile), chert, and intraclasts of microcrystalline siderite. The relative abundance of quartz types is $Qm_{79.7}Qp2\text{–}3_{9.2}Qp > 3_{11.1}$ (Fig. 4C). CL shows both blue (more common in the Middle TAGI than in the Upper TAGI) and dark red/brown (more common in the Upper TAGI than in the Middle TAGI) quartz grains.

4.3. Diagenetic phases

Significant diagenetic phases in the TAGI sandstones include illite, kaolin, pyrite, K-feldspar, dolomite, magnesite–siderite, quartz, anhydrite, barite and bitumen (Fig. 5).

4.3.1. Grain-coating illitic clay

The coatings consist of illitic clay platelets arranged tangentially to, and in places partially detached from, grain surfaces (Fig. 6). Usually, the coats are thicker in

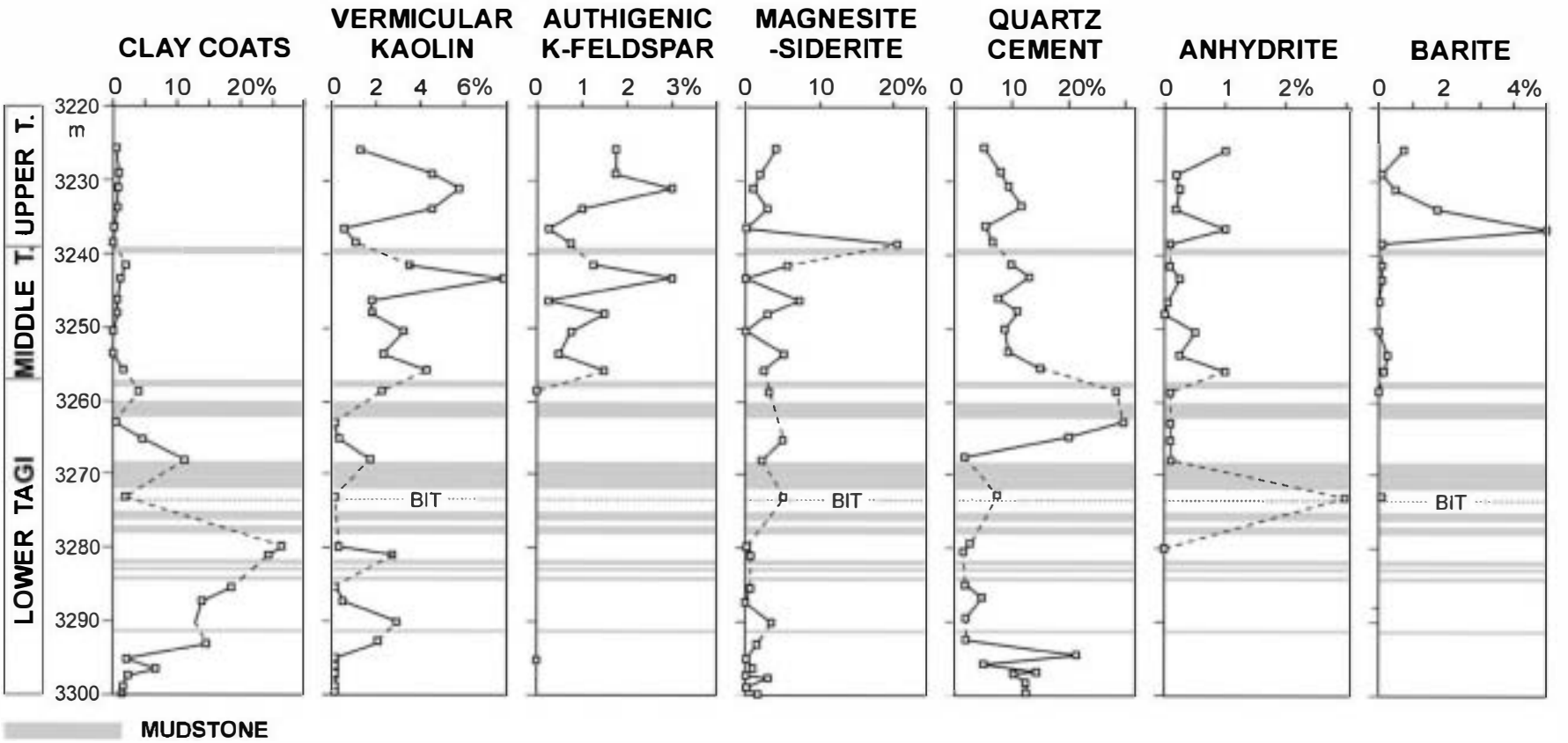

Fig. 5. Vertical distribution of selected diagenetic phases in the cored section studied, showing the location of mudstone intervals and the bitumen-cemented interval (BIT).

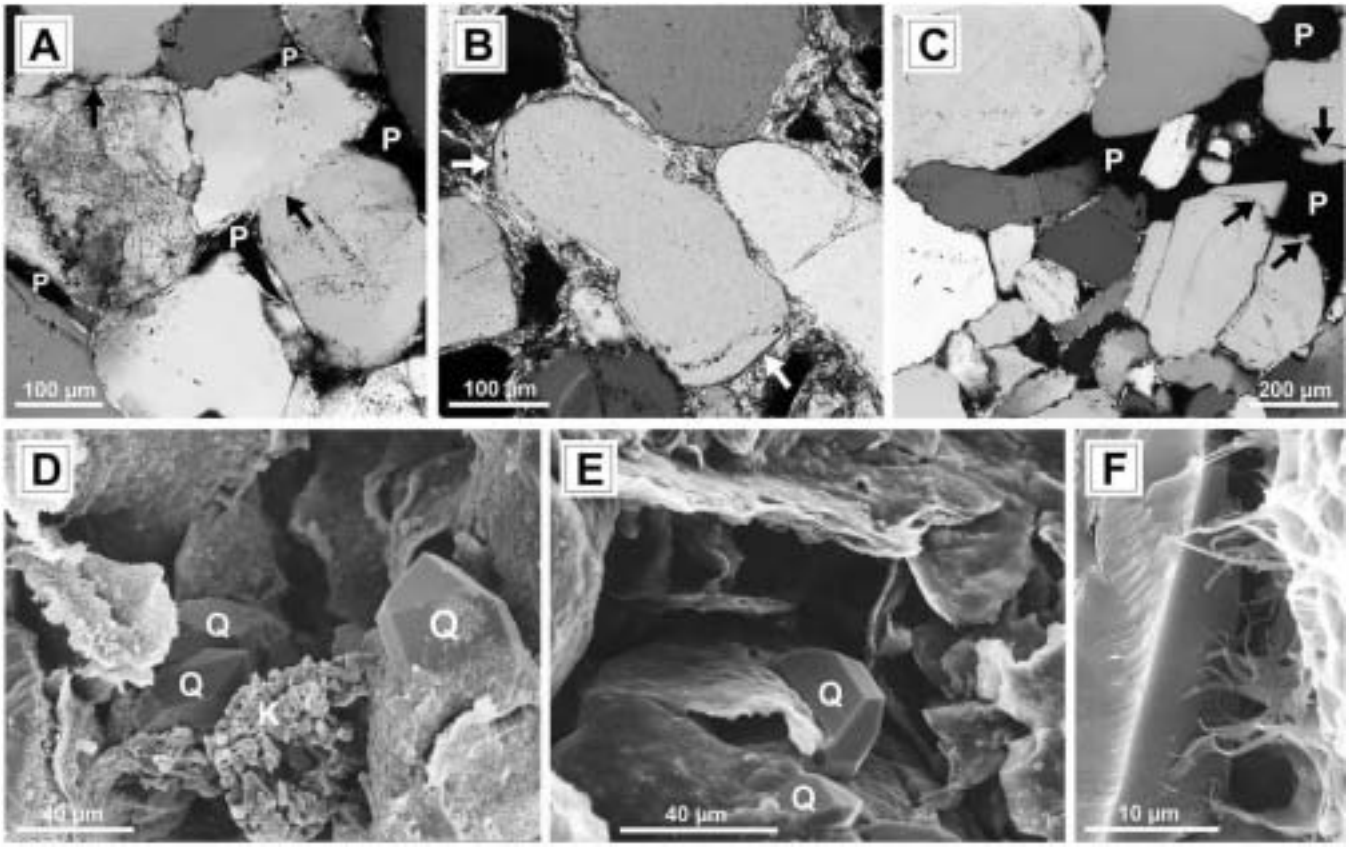

Fig. 6. Petrography of grain-coating illitic clay in Lower TAGI sandstones. A: cross-polarized-light photomicrograph showing relatively thin illitic coatings on quartz grains. The coats have inhibited quartz overgrowth, preserving some primary porosity (P), but have favored chemical compaction as revealed by the predominance of intergranular sutured contacts (arrows). B: cross-polarized-light photomicrograph showing thick illitic coats, whose formation predated compaction. Note the presence of inherited abraded overgrowths on detrital quartz grains beneath illitic coats (arrows). C: cross-polarized-light photomicrograph of a typical Lower TAGI sandstone. The presence of thin illitic grain coats has favored intense chemical compaction, resulting in tight packing (lower part of the image). Porosity (P, black) mainly consists of oversized pores probably related to the dissolution of feldspar grains. Although pores are generally bordered by grain-coating illite and thus protected from quartz cementation, some quartz outgrowths (arrows) have formed where clay coats were thinner. D and E: SEM images showing thick illitic coatings bordering primary porosity. The coats are partially detached from grain surfaces and some quartz outgrowths (Q) have formed where detrital surfaces were not completely covered by illite. Pore-filling kaolin (K) is locally present. F: SEM image showing authigenic fibrous illite overgrowing a detrital coating (to the right) and being partially enclosed in quartz cement (to the left).

sandstones containing abundant mud intraclasts than in sandstones with few mud intraclasts. In laminated sandstones, coatings preferentially occur in the finer-grained laminae. These textural characteristics are consistent with an infiltrated (ultimately detrital and/or pedogenic) origin for the grain-coating illite (cf. Moraes & De Ros, 1990; Pittman, Larese, & Meald, 1992; Walker, Waugh, & Crone, 1978). XRD reveals that illite is associated with traces of mixed-layered illite/smectite (in the Lower TAGI) and chlorite (in the Middle–Upper TAGI). In the Lower Tagi, some illitic coatings are texturally similar to smectite, suggesting a smectitic precursor (cf. Morad, Ben Ismail, De Ros, Al-Aasm, & Serrihini, 1994) that would have been partially to completely illitized during diagenesis. The presence of mixed-layered illite/smectite supports this hypothesis. Grain-coating illitic clays are abundant in the Lower TAGI, though with an irregular stratigraphic distribution (Fig. 5) that is facies controlled. In the Middle–Upper TAGI, grain-coating illitic clays are uncommon, and coats are usually thin and discontinuous.

4.3.2. Grain-coating kaolin

In samples from subunit TL2, kaolin (i.e. dickite and/or kaolinite, sensu Ehrenberg, Aagaard, Willson, Fraser, & Duthie, 1993) forms felt-like mats of platy crystals arranged tangentially around grains, locally occluding intergranular porosity. This type of kaolin is commonly mixed with illitic clays, and in this case CL helps in their discrimination. Similar to illitic coats, the formation of kaolin coatings predates compaction. Locally, the kaolin masses are red-stained due to adsorbed Fe-oxides. XRD indicates that the kaolin mineral is mostly the dickite polytype. Sandstones containing grain-coating kaolin are relatively friable, white to reddish, typically contain root traces, and have low macroporosity and very low permeability.

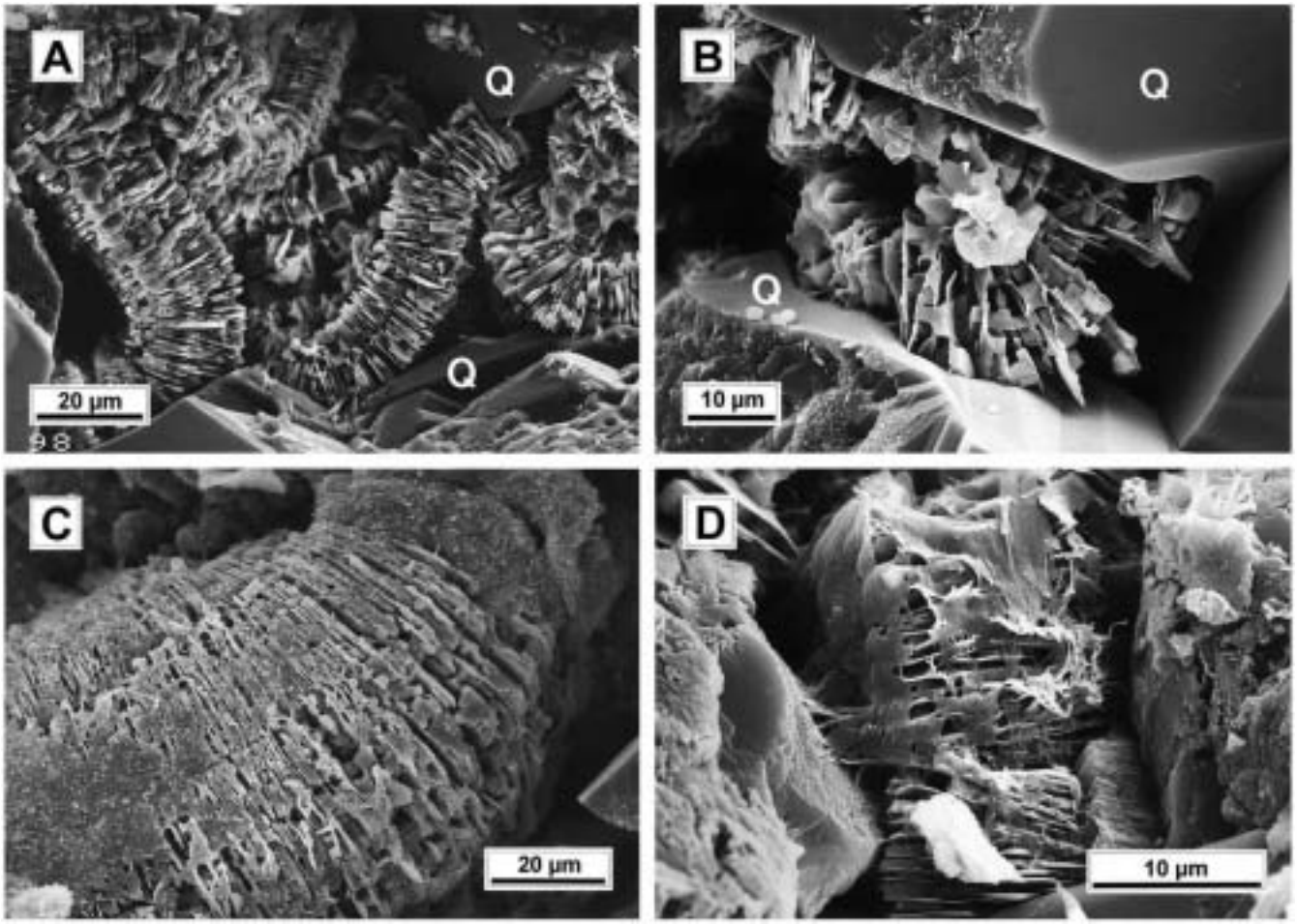

Fig. 7. SEM images of vermicular kaolin. A and B: pore-filling vermicular kaolin. Most kaolin crystals show the blocky habit typical of dickite, and enclose remnants of thin kaolinite platelets. B: quartz overgrowths enclose, and hence postdate the precipitation of kaolin. C and D: kaolinite-dickite vermicules partially covered by late-diagenetic fibrous illite.

4.3.3. Vermicular kaolin

Kaolin with the characteristic vermicular or 'booklet' texture (Fig. 7) occurs both as pore-filling cement and as a replacement product of feldspars. Most individual kaolin crystals show the blocky habit typical of dickite (Fig. 7B; cf. Ehrenberg et al., 1993; Morad et al., 1994). In fact, XRD analysis of a randomly oriented clay fraction from a selected sample confirmed the presence of dickite. Dickite most likely replaced pre-existing kaolinite, as suggested by the presence of thin kaolin platelets, interpreted to be remnant kaolinite (cf. Morad et al., 1994), enclosed within or between dickite crystals (Fig. 7). Because of its general replacement by dickite, it is difficult to place precipitation of the original kaolinite in the paragenetic sequence. However, kaolinite must have formed relatively early in the paragenesis, because it is enclosed by magnesite–siderite, quartz, and sulfate cements. This is consistent with the observation that some kaolin masses, that seem to be replacive of feldspars, have been deformed by mechanical compaction.

Vermicular kaolin is ubiquitous in the studied sandstones, but it is particularly common in the Middle–Upper TAGI (Fig. 5), due to the higher original feldspar content in the sandstones from these units. Here, XRD indicates that, after illite, kaolin is the second most abundant clay mineral.

4.3.4. Pyrite

Pyrite occurs in minor amounts (<1 vol%), especially in Middle and Upper TAGI sandstones, where it forms mm-scale poikilotopic patches, preferentially within argillaceous grains and laminae, as well as within plant fragments. Pyrite is locally abundant along the contacts between sandstone beds and underlying mudstone, where it occurs as nodules of up to 1 cm in size (Terence Eschner, pers. comm.). Locally, pyrite also occurs as isolated pyritohedrons, up to 50 µm in diameter, that rim detrital grains and are enclosed in Fe-dolomite cement.

4.3.5. Dolomite

Dolomite occurs as poikilotopic crystals and, less frequently, as mosaics of rhombic crystals. Dolomite crystals usually contain abundant fluid inclusions which give the

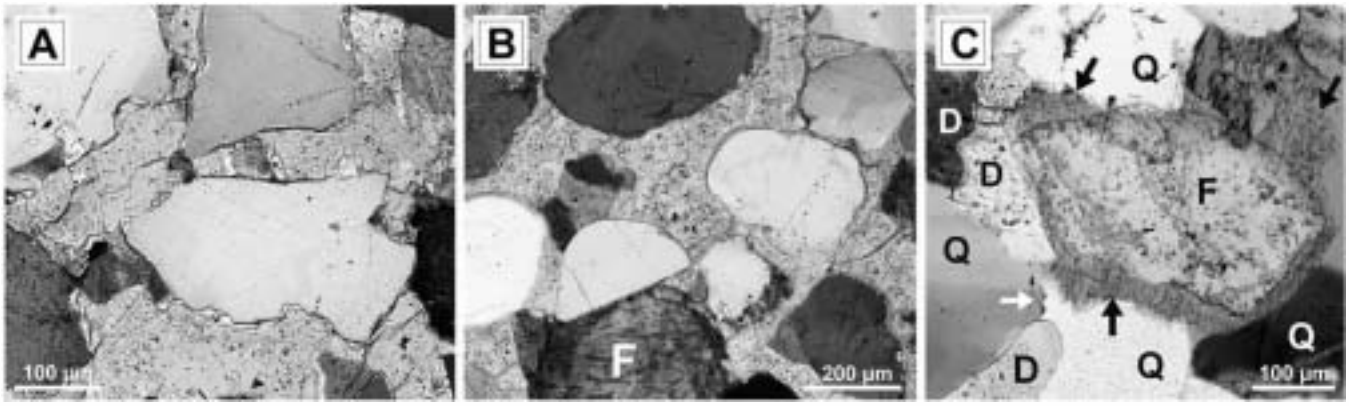

Fig. 8. Transmitted-light petrography of Fe-dolomite and feldspar cements. A and B: precompactional fluid-inclusion-rich Fe-dolomite cement completely occluded the intergranular porosity. High intergranular volumes indicate that cementation occurred prior to significant compaction. Feldspar (F) and quartz grains enclosed in the dolomite are devoid of overgrowths, indicating the early paragenetic timing of the dolomite. C: feldspar cement (black arrows) overgrowing detrital K-feldspar (F). Fe-dolomite (D) impeded, and hence predated, feldspar overgrowths. In turn, feldspar overgrowths impeded, and hence predated, growth of quartz (Q) cement (white arrow).

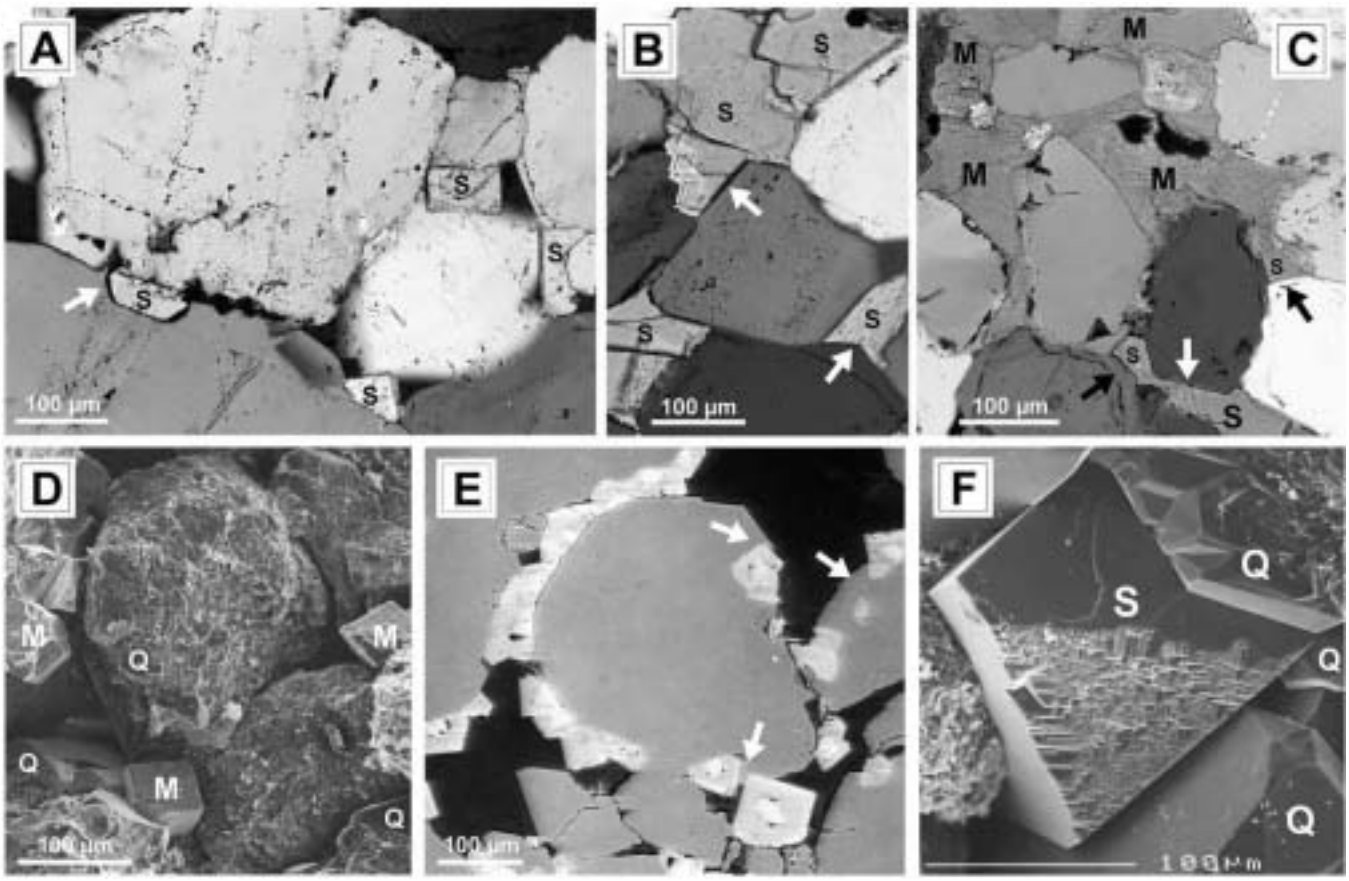

Fig. 9. Petrographic aspects of magnesite-siderite cement. A: cross-polarized-light photomicrograph showing precompactional magnesite–siderite rhombs (S) enclosed in quartz overgrowths (arrow). B: postcompactional siderite (S) postdating euhedral quartz overgrowths (arrows). C: magnesite–siderite poikilotopic crystal. In the upper part of the image, magnesite cement (M) is seen to preserve high intergranular volume, and the enclosed quartz grains lack overgrowths. Younger siderite cement (S) in lower part of the image) postdates compaction and euhedral quartz overgrowths (arrows). D: SEM image showing precompactional magnesite–siderite rhomboedra (M) partially enclosed in quartz overgrowth cement (Q). E: BSE image of a similar area to D revealing zonation of magnesite–siderite rhombs (for details see Fig. 10B); arrows mark quartz cement. F: SEM image showing a relatively large magnesite–siderite crystal (S). The youngest growth zone of the crystal is composed of siderite (pistomesite) that postdates quartz overgrowth (Q).

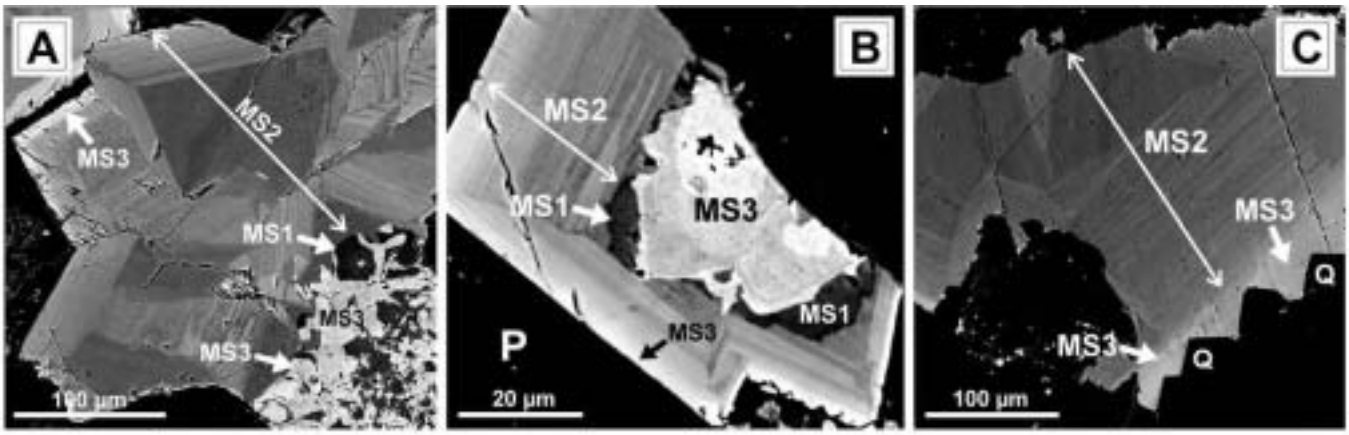

Fig. 10. BSE images illustrating magnesite–siderite cement stratigraphy: A: Breunnerite (dark grey, MS1, lower right corner) is extensively replaced by pistomesite (bright, MS3), resulting in a mottled aspect. MS2 breunnerite (medium gray) forms the bulk of this poikilotopic crystal and shows a combination of sector and concentric zoning. In the upper left corner of the image, pistomesite (bright, MS3) locally overgrowths MS2. B: Breunnerite (dark, MS1) originally formed the core of this crystal, but it is now selectively replaced by late-stage pistomesite (MS3, bright), which also constitutes the rim of the crystal. A prominent corrosion surface separates MS1 from MS2, which shows fine-scale concentric zoning. C: MS2 covers detrital quartz (in black) surfaces lacking overgrowths, whereas MS3 (BSE—lighter, arrows) encloses, and hence postdates, euhedral quartz overgrowths (Q).

crystals a turbid aspect in transmitted light (Fig. 8A). A high Fe content of the dolomite is indicated by its blue staining with potassium ferricyanide and was confirmed by EDX analysis. The intergranular volumes (IGV; sensu Lundegard, 1992) within dolomite-cemented domains usually exceed 40% (e.g. Fig. 8B), which indicates precipitation during an early stage of burial (a few hundred meters at most; cf. Gluyas & Cade, 1997). These high IGVs resulted from filling of primary intergranular porosity during shallow burial and are not apparently influenced by replacement of grains or from filling of secondary pores. This is because the grains enclosed within dolomite usually do not show signs of replacement and dolomite has not been observed filling secondary pores. Dolomite predates the precipitation of feldspar (Fig. 8C), quartz, and magnesite–siderite cements, which normally overgrow the outer edges of the dolomite crystals. Anhydrite and barite commonly replace, and hence postdate, dolomite cement. Dolomite is common throughout the Middle–Upper TAGI section of well B, where assessed contents range from ~2 to ~4 vol%. However, no dolomite has been observed in well A or in the Lower TAGI section of well B.

4.3.6. K-feldspar overgrowths

K-feldspar overgrowths are restricted to Middle–Upper TAGI sandstones (Fig. 5), where assessed contents range from 0.5 to 3%, averaging 1.3%. K-feldspar overgrowths are commonly partially dissolved, and restored authigenic K-feldspar contents range from 1 to 4.25%, averaging 2.2%. K-feldspar overgrowths are relatively early in the paragenesis (Fig. 8C). They predate significant compaction and also magnesite–siderite, quartz, and sulfate cements.

4.3.7. Magnesite–siderite

Magnesite–siderite is a common pore-filling cement and locally has replaced feldspars and mud intraclasts. It occurs both as isolated rhombic crystals and as poikilotopic patches (Fig. 9). Three main generations of magnesite–siderite (MS1, MS2 and MS3) have been distinguished under BSE (Fig. 10). MS1 is composed of Fe-rich magnesite (breunnerite) with an average composition of

Fig. 11. Transmitted-light petrography of quartz, anhydrite and barite cements. A: euhedral syntaxial quartz overgrowths bordering primary and oversized (O) pores (blue), in a quartz arenite from subunit TL1. B: example of a Lower-TAGI sandstone, in which grain-coating illite has largely impeded quartz overgrowth and thus accounted for the preservation of significant primary porosity (blue); minor amounts of quartz cement tend to occur as localized outgrowths (arrows). C: middle-TAGI sandstone with authigenic overgrowths on feldspar grains (F) that have partially impeded quartz overgrowths (black arrows). Porosity (blue) is mostly primary in origin, with additional honey-comb porosity (white arrows) resulting from (authigenic) feldspar dissolution. D: postcompactional magnesite–siderite cement (S) replacing feldspar overgrowths (white arrow). Black arrows indicate areas where a first generation of quartz overgrowth is seen to predate magnesite siderite cement. Note that quartz overgrowths are markedly thicker where magnesite–siderite is absent. E: poikilotopic anhydrite cement (brown–blue interference colors) with replacement features along the margins of enclosed quartz grains and magnesite–siderite (S) cement. Arrows point to corroded inclusions of magnesite–siderite. F: poikilotopic anhydrite enclosing euhedral quartz overgrowths (arrows). G: poikilotopic anhydrite enclosing quartz grains with scarce and irregularly developed overgrowths. The anhydrite preferentially replaced magnesite–siderite cement, as demonstrated by the occurrence of inclusions (black arrows) inside anhydrite crystals. H: poikilotopic barite cement (gray interference colors, B) has replaced dolomite (D), as indicated by the presence of corroded dolomite inclusions (arrows) within barite. I: fluid-inclusion-rich poikilotopic barite cement (gray interference colors, B) replace extensively the margins of the enclosed quartz grains.

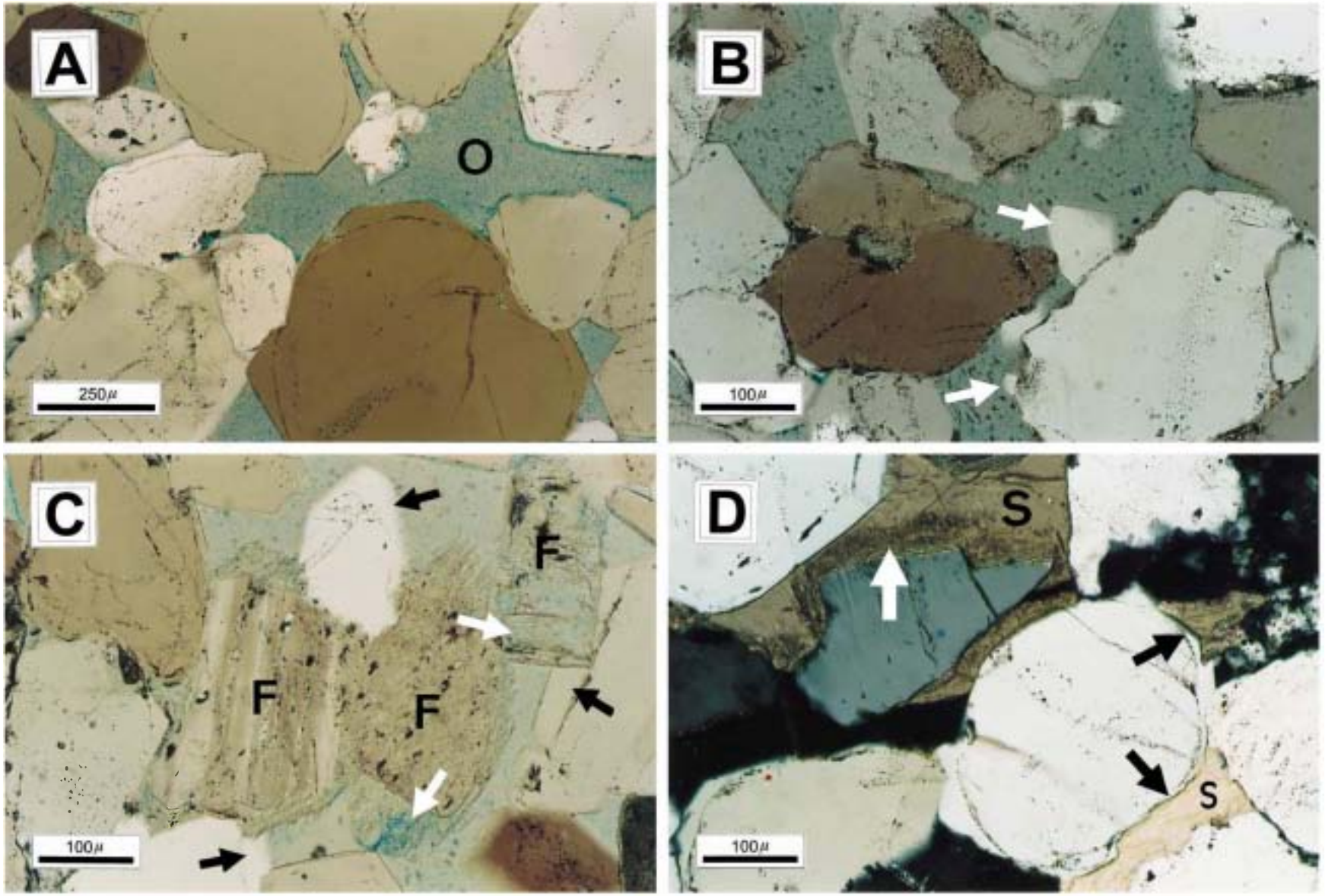

Fig. 11.

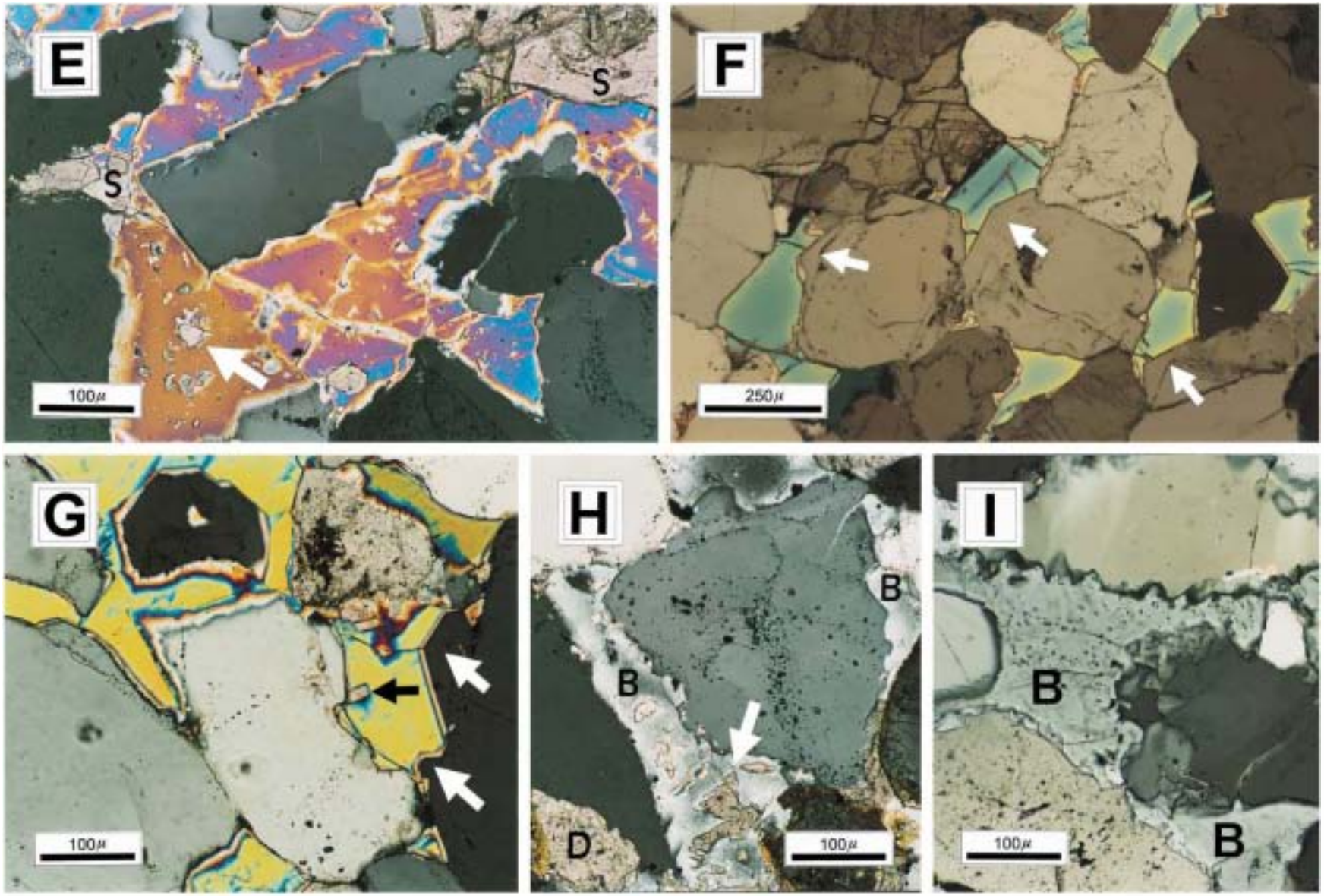

Fig. 11. (*continued*).

$(Ca_{0.005}Mg_{0.664}Fe_{0.319}Mn_{0.012})CO_3$ ($N = 44$). It is relatively dark in BSE and is commonly partially replaced by younger siderite zones, resulting in a mottled BSE aspect (Fig. 10A). A corrosion surface separates MS1 from MS2 (Fig. 10B). MS2 is mainly composed of Fe-rich magnesite (breunnerite), with an average composition of $(Ca_{0.005}Mg_{0.53}Fe_{0.445}Mn_{0.02})CO_3$ ($N = 94$), and shows concentric and sector zoning (Fig. 10A–C). MS2 can be subdivided into subzones whose Mg content decreases progressively towards the younger subzones, with the latest one composed of Mg-rich siderite (pistomesite). MS3 is entirely composed of Mg-rich siderite (pistomesite) with an average composition of $(Ca_{0.004}Mg_{0.364}Fe_{0.616}Mn_{0.016})CO_3$ ($N = 73$). MS3 has a relatively bright BSE aspect, may overgrow MS2 and, more commonly, infills irregular areas within MS1 or replaces extensively MS1 (Fig. 10B).

MS1 predates significant compaction and quartz overgrowth, but locally infills feldspar molds and thus postdates some feldspar dissolution. MS2 postdates much compaction and, at least in part, predates quartz overgrowth. MS3, however, engulfs, and hence postdates, quartz overgrowth (Fig. 10C). MS3 is postdated by anhydrite and barite and shows no signs of dissolution, as it displays euhedral crystal faces where it borders porosity.

Magnesite–siderite is present throughout all the studied sections, but with a tendency to gradually decrease in abundance downward (Fig. 5). Its abundance is higher in well B, but this datum must be treated with caution, as cutting samples tend to be biased towards mechanically more resistant lithologies.

4.3.8. Quartz cement

Quartz cement mainly occurs as syntaxial overgrowths (Fig. 11A). In clay-coat-rich sandstones it also occurs as syntaxial outgrowths (Fig. 11B) as a result of partial inhibition of cement growth by grain-coating clay. Quartz cementation postdates the precipitation of dolomite, feldspar (Fig. 11C,D), kaolin, much magnesite–siderite (MS1 and MS2) (Figs. 10C and 11D) and, in part, chemical compaction. Some quartz overgrowths adjacent to feldspar molds show rhombohedral embayments related to the dissolution of feldspar overgrowths, indicating that some feldspar dissolution postdated quartz overgrowth (Fig. 11C). At least two generations of in-situ (i.e. non-detrital) quartz cement can be distinguished under CL. The first generation luminesces reddish and the second is virtually non-luminescent. The second generation is found to occur as thicker layers in stratigraphically lower rocks, particularly below a bitumen-cemented interval (see below).

Quartz is generally the most abundant cement, averaging 10 vol%. In the Lower TAGI, quartz cement abundance is highly variable (1.5–30 vol%) and inversely correlates with the content in grain-coating clay (Fig. 5). In the Middle–Upper TAGI, the percentage of quartz cement is less variable (5–14.75%) and does not show any significant correlation with clay content. If the samples with packstone texture are excluded, the average contents in quartz cement are 13.1 (Lower TAGI) and 9.2 vol% (Middle–Upper TAGI).

4.3.9. Anhydrite and barite

Anhydrite cement typically forms submillimetric poikilotopic patches with replacement features affecting the margins of enclosed framework grains and cements (Fig. 11E–G). Anhydrite preferentially replaces feldspars, argillaceous grains and carbonate cements. This is indicated by the common occurrence of corroded inclusions of these minerals enclosed in the anhydrite crystals (Fig. 11E). Anhydrite postdates compaction and all the aforementioned authigenic phases. Also, anhydrite can be seen to enclose thick, in-situ quartz overgrowths (Fig. 11F). However, elsewhere, quartz grains embedded in the anhydrite show only minor (Fig. 11G) or no overgrowth at all (Fig. 11E). This is because anhydrite preferentially replaces argillaceous pseudomatrix and dolomite or magnesite–siderite cements, as demonstrated by the common occurrence of carbonate and clay inclusions inside anhydrite crystals.

Barite has a morphology identical to anhydrite, and usually forms patches of fluid-inclusion-rich poikilotopic crystals that tend to replace extensively the margins of the enclosed detrital grains (Fig. 11H,I). Barite encloses and corrodes, hence postdates, dolomite (Fig. 11I), K-feldspar, kaolinite, magnesite–siderite, and quartz cements. Barite is invariably associated with anhydrite, and both sulfates commonly co-exist within the same patches where they do not corrode mutually.

Barite is exclusively observed in Middle–Upper TAGI samples (Fig. 5), where it occurs in minor amounts (up to 3.75 vol% in well A, and up to 4 vol% in well B). Similar to barite, anhydrite occurs in virtually all the Middle–Upper TAGI samples (up to 1 vol% in well A, and up to 1.75 vol% in well B). However, anhydrite is absent in most of the samples from the Lower TAGI except for those from the uppermost part of this unit in well A (Fig. 5).

4.3.10. Minor authigenic phases

Minor amounts of late-diagenetic fibrous illite occur throughout the entire TAGI succession. It forms hair- or thread-like crystals that have replaced or intergrown with previous authigenic or detrital clays (Fig. 6E). It also forms pore-bridges overlying, and locally partially enclosed within, quartz cements (Fig. 6F). Illite preferentially replaces or intergrows with vermicular kaolin (Fig. 7D).

Late-diagenetic bitumen occurs locally. It forms either pore-filling masses containing abundant vesicles and shrinkage cracks or thin, dark brown coatings on surfaces of quartz overgrowths. Significant bitumen (10.25 vol%) is restricted to one specific level, where it almost completely occludes porosity. This level is located near to the interpreted present OWC. Minor amounts of bitumen also occur immediately above this level. Elsewhere in the studied sections, bitumen is absent.

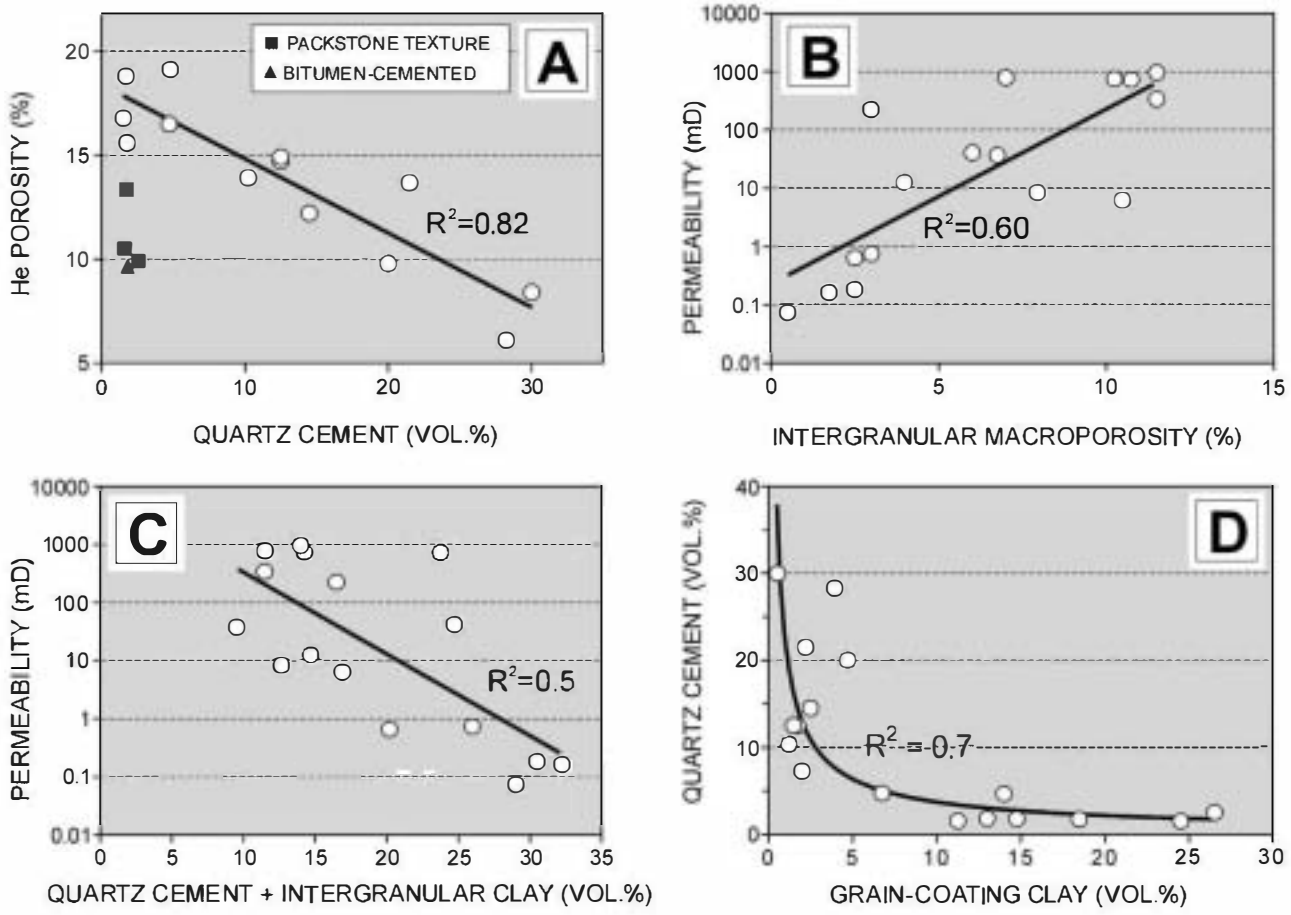

Fig. 12. Plots of porosity vs. quartz cement (A), permeability vs. intergranular macroporosity measured in thin section (B), permeability vs. quartz cement + intergranular clay (C) and quartz cement vs. grain-coating clay (D), for Lower TAGI sandstones.

4.4. Reservoir properties

Primary intergranular pores, bordered by quartz overgrowths (Fig. 11A) or clay coats (Fig. 11B), are the predominant pore type in all the sandstones examined. Secondary moldic and honeycomb pores, related to the dissolution of detrital and authigenic feldspar, are also present (Fig. 11C). Secondary porosity is of very minor significance in the Lower TAGI, because of its very low initial feldspar contents. However, in the Middle–Upper TAGI secondary porosity contributes significantly (2–4.75%) to total porosity.

4.4.1. Lower TAGI

Throughout the Lower TAGI, reservoir quality is very variable and is mainly controlled by the content in grain-coating clay and quartz cement. High contents in grain-coating clay result in sandstones with packstone texture (e.g. subunit TL2), which have the lowest thin-section (TS) porosities (<3%) and permeabilities (<1 mD). Overall, He porosity is inversely correlated with quartz cement volume, especially if the samples with packstone texture and those extensively cemented by bitumen are excluded ($r^2 = 0.82$, Fig. 12A). Permeability is poorly correlated with grain size ($r^2 = 0.34$) and clay content ($r^2 = 0.23$), and moderately correlated with intergranular TS porosity ($r^2 = 0.6$; Fig. 12B). Because this porosity is in turn mainly controlled by the combined effect of quartz cement and grain-coating clay, there is also a moderate correlation between permeability and the sum of quartz cement and grain-coating clay ($r^2 = 0.5$; Fig. 12C).

The abundance of quartz cement in the Lower TAGI appears to be controlled primarily by grain-coating clay. There is a trend of decreasing quartz cement with increasing grain-coating clay (Fig. 12D). However, in clay-coat-poor sandstones (i.e. <5 vol% of grain-coating clay), quartz cement varies widely (7.5–30 vol%). Some of this variation may be related to the proximity of clay-rich facies, particularly towards the top of the Lower TAGI. Here, in clay-coat-poor sandstones adjacent to mudstone beds, quartz cementation is extensive (28–30 vol%) (Fig. 13). Elsewhere in the Lower TAGI, quartz cementation in clay-coat-poor sandstones is less extensive but variable (7.5–21.5 vol%), and this variation is not clearly related to the proximity of clay-rich facies. In particular, this applies to the sandstones of subunit TL1, which have the best reservoir quality. They have relatively high He porosities (typically 14–16%), in spite of the abundant

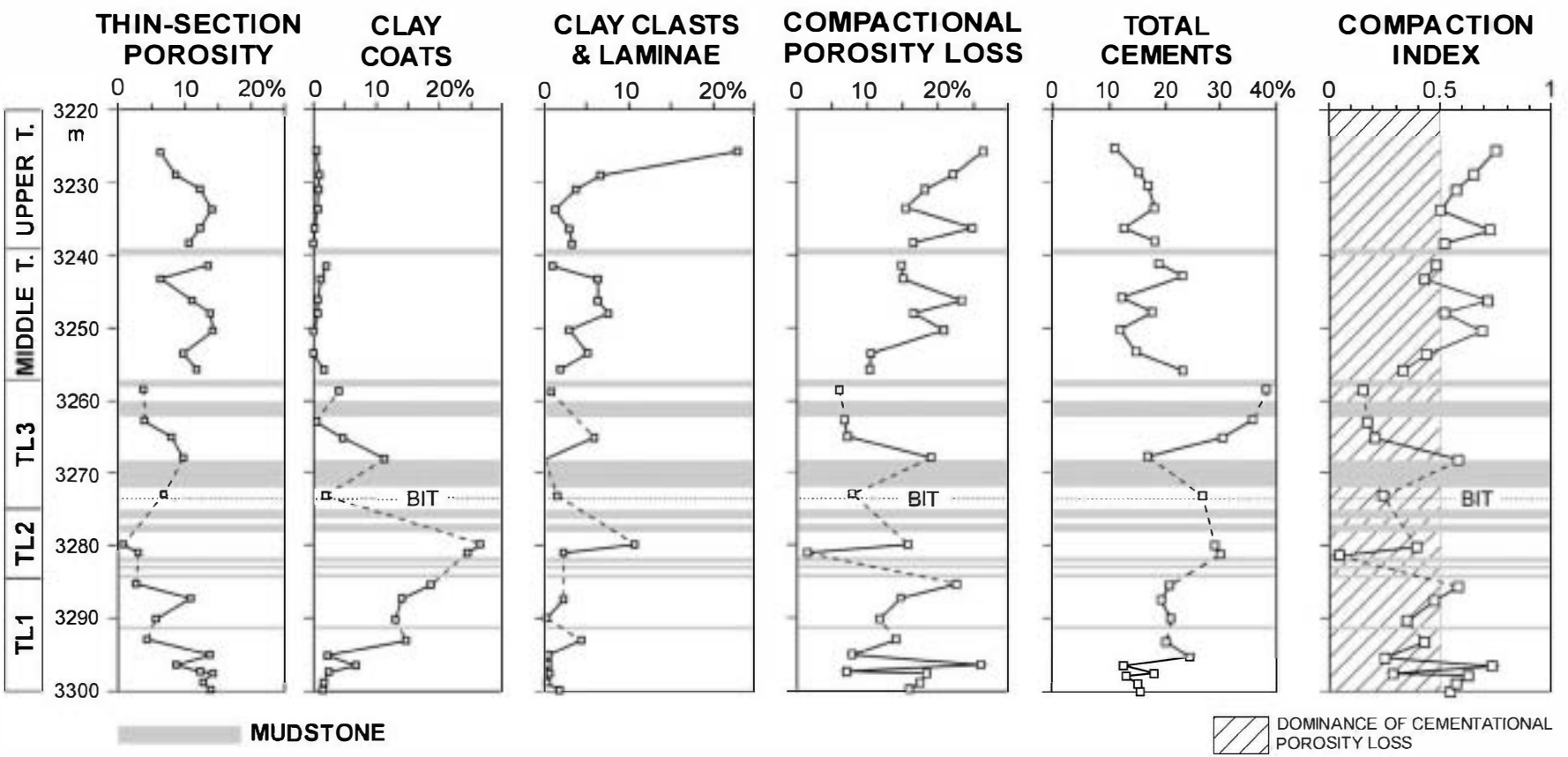

Fig. 13. Vertical distribution of porosity and other selected parameters in the studied cored section, showing the location of mudstone intervals and the bitumen-cemented interval (BIT).

quartz cement (typically between 12.5 and 21.5 vol%). Moreover, their relative coarse grain size and the predominance of well-connected intergranular macropores, result in relatively high permeabilities. In subunit TL1, the porosity–permeability pattern is somewhat different from the rest of the Lower TAGI: in subunit TL1, the correlation between porosity and permeability is better ($r^2 = 0.6$), and permeabilities are higher and less variable than in the rest of the Lower TAGI.

If the samples with packstone texture are excluded, the average He porosity is significantly lower in the Lower TAGI than in the Middle–Upper TAGI (13.7 vs. 16.6%, respectively). Interestingly, the average content in quartz cement in these sandstones is 4% higher for the Lower TAGI than for the Middle–Upper TAGI, which suggests that quartz cementation is one of the main causes of the overall lower porosity of the Lower TAGI reservoir sandstones relative to those of the Middle–Upper TAGI.

4.4.2. Middle–Upper TAGI

In the studied cored section, reservoir quality is relatively homogeneous across this interval. Porosity slightly decreases up-section, probably as a result of increasing detrital-clay content. The lowest porosities relate to elevated abundances of detrital clay (mud intraclasts and drapes) and thus to higher degrees of compaction (see below). TS porosities usually vary between 9.5 and 14.2% (Fig. 13). He porosities exceed TS porosities typically by 2–10% ($r^2 = 0.6$), reflecting the presence of significant microporosity, which is contained within authigenic and detrital clays. Permeability is poorly correlated with He porosity ($r^2 = 0.4$), and shows very poor correlations with grain size ($r^2 = 0.16$), clay content ($r^2 = 0.19$) and quartz cement ($r^2 = 0.18$). Similar to porosity, permeability also tends to decrease up-section and the lowest permeabilities are associated with the highest abundances in detrital clay. The highest permeabilities correlate with coarser-grained lithologies (medium-grained sandstones) and also with peaks in magnesite–siderite abundance.

In well B, log-deduced reservoir quality in the Middle–Upper TAGI section is significantly lower than in well A. Because this variation is not related to differences in detrital composition, grain size or clay content, it might be related to differences in the degree or type of cementation. In fact, the total volume of the cements is significantly higher in well B (23–30%) than in well A (11–22%). This variation is mainly due to magnesite–siderite (mean values: 4 vol% in well A vs. 12 vol% in well B) and sulfate (mean values: 1 vol% in well A vs. 4 vol% in well B) cements. However, these data must be treated with caution, as cutting samples tend to be biased towards more indurated lithologies. Because dolomite cement is only present in well B, it has contributed to the lower porosity in this well relative to well A.

4.4.3. Compaction versus cementation in porosity reduction

In matrix-free sandstones, compactional porosity loss (COPL, sensu Lundegard, 1992; initial porosities assessed after Beard and Weyl, 1973) ranges from 7 to 26%, averaging 16%, and is closely related to the content in depositional clay (intraclasts, laminae, and grain coats) (Fig. 13). Moreover, dissolution features (sutured contacts and stylolites) are more abundant in clay-rich sandstones and in the clay-rich laminae of laminated sandstones, where porosity is severely reduced by compaction (Fig. 6A). In the Middle–Upper TAGI, COPL ranges 10–26% and shows a poor correlation with detrital clay content ($r^2 = 0.3$) (Fig. 13). The lowest COPL values (~10%) are found towards the base, where they are related to the presence of precompactional magnesite cement (Fig. 9E), which presumably acted as a framework-strengthening cement that inhibited mechanical compaction. In the Lower TAGI, COPL is more variable and is controlled largely by the distribution of grain-coating clay (Fig. 13).

The total volume of the cements is higher in the lower TAGI than in the Middle–Upper TAGI (Fig. 13). The higher cement volumes of the Lower TAGI are related to greater abundances of quartz cement and grain-coating clay. The compaction index (ICOMP, sensu Lundegard, 1992) allows the assessment of the relative importance of compaction versus cementation in the reduction of the original porosity. By plotting of ICOMP versus depth (Fig. 13) it appears that in the Middle–Upper TAGI compaction is more important than cementation in reducing porosity, whereas in the Lower TAGI the contrary applies.

5. Discussion

5.1. Provenance

The Lower TAGI sandstones had their source in siliciclastic sedimentary rocks, as indicated by their high compositional maturity, the predominance of monocrystalline quartz, which commonly bears inherited overgrowths, the scarcity of feldspar and mica, and the presence of sandstone rock fragments. In a QtFL diagram (Dickinson, 1985) (Fig. 4D), the Lower TAGI sandstones plot at the Qt pole, which is consistent with a 'craton interior' provenance type (Dickinson, op. cit.). Source rocks were likely Carboniferous and Devonian siliciclastics, which subcrop the Hercynian unconformity in the central Berkine Basin (Fig. 2). Pre-Devonian siliciclastics could have been additional sources, as they were also exposed during the Triassic along major paleohighs (Echikh, 1998). The presence of minor quantities of quartz grains showing bright red CL is consistent with a subordinate volcanic contribution (Owen, 1991). It is unclear however if this contribution reflects penecontemporaneous volcanism or if volcanic quartz was recycled from Paleozoic strata.

By contrast, the Middle–Upper TAGI sandstones derived

mainly from metamorphic terrains, presumably from the Hoggar Massif to the south. Evidence for such kind of source terrain includes the presence of significant amounts of feldspar, mica, and low-grade metamorphic rock fragments, and the relative high percentage of polycrystalline quartz. The overall predominance of brown-red luminescent quartz is also consistent with a metamorphic source (cf. Matter & Ramseyer, 1985; Owen, 1991). Plotted in a QtFL diagram (Dickinson, 1985) (Fig. 4D), the detrital composition of the Middle–Upper TAGI sandstones indicates a provenance related to the erosion of continental blocks ('transitional continental' field in Dickinson's, op. cit., diagram).

Near the base of the Middle TAGI, blue-luminescent quartz prevails, consistent with an influence of plutonic source rocks (cf. Owen, 1991). This inference is further supported by the local presence of granitic rock fragments. An additional influence of sedimentary source areas is evidenced by the presence of rare sandstone rock fragments. The influence of plutonic sources could have been related to the erosion of granitic basement in the Dahar paleohigh (cf. Morad et al., 1994), which represents the northern limit of the Berkine Basin.

The marked difference in detrital composition between the Lower and Middle–Upper TAGI is thus caused by a change in provenance. This change may reflect an unroofing sequence related to progressive erosion of the flanks of the Hoggar Massif. Alternatively, the change in composition may have been caused by a variation in source area. In this case, the Lower TAGI could derive from local exposures of Paleozoic siliciclastics, whereas the Middle–Upper TAGI could mainly derive from more distant sources, such as the metamorphic terrains of the Hoggar massif.

5.2. Origin of the authigenic phases

5.2.1. Vermicular kaolin

In the studied sandstones, vermicular kaolin usually shows the blocky habit typical of dickite, whose presence is confirmed by XRD. Based on the presence of thin kaolin platelets interleaved with the blocky kaolin crystals (Fig. 7), dickite is interpreted to have replaced, at least in part, previously formed kaolinite. The paragenetic timing of this kaolinite is uncertain, but petrographic observations suggest a shallow burial origin (see above).

Because most kaolin occurs as sand-grade patches or within partly dissolved K-feldspar grains, the original precipitation of kaolinite is interpreted to have been related to the dissolution of feldspar grains. Dissolution of feldspar and concomitant precipitation of kaolinite requires pore water with low (K^+, Na^+)/H^+ ratios and a mechanism to remove excess silica and (K^+, Na^+) from the system. Fluxing by freshwaters at shallow depths is a likely explanation for such kind of alteration of feldspars to kaolinite (Bjørlykke, 1998). Since the TAGI sandstones are fluvial in origin, they were fluxed by meteoric water immediately after deposition and also probably during the development of the subaerial unconformities that occur on top of the TAGI subunits.

Alternatively, acids from maturing hydrocarbon source rocks may have induced feldspar dissolution and, if K^+ was exported (e.g. to adjacent mudrocks), the subsequent precipitation of kaolinite and quartz (e.g. Worden & Barclay, 2000). However, if it is correct that kaolinite originally precipitated during shallow burial, this mechanism seems unlikely because organic matter maturation and clay-mineral reactions in mudrocks would require higher temperatures than those normally expected at shallow depths.

As discussed above, the original kaolinite was replaced by dickite. Such a replacement requires relatively high minimum temperatures (80–130 °C) and pore waters with low K^+/H^+ ratios, since otherwise illite would form (Ehrenberg et al., 1993). A possible source of H^+ during burial diagenesis is the input of acids from maturing source rocks. Because K-feldspars are abundant in the Middle–Upper TAGI, the input of acids would probably result in their dissolution and the subsequent release of K^+. Therefore, in order to keep low K^+/H^+ ratios, K^+ should have been removed from the system, for instance by exporting it to adjacent mudrocks (cf. Thyne, Boudreau, Ramm, & Midtbø, 2001)

As deduced from SEM observations, dickitization is postdated by a late phase of illitization. The illitization of kaolin is favored by high K^+/H^+ ratios and low water-to-rock ratios (Morad, Ketzer, & De Ros, 2000). In sandstones, the K^+ required for late-diagenetic illitization is normally supplied by the dissolution of K-feldspars (Bjørlykke, 1998). In the TAGI sandstones, petrography shows that there was a late-stage phase of dissolution of detrital and authigenic K-feldspars that could have caused the partial illitization of kaolin. Illitization of kaolin in sandstones is favored at relatively high temperatures (normally above 100 °C: Wilson & Stanton, 1994) and by oil emplacement, which reduces the mobility of K^+ and thus prevents its possible export to adjacent mudstones (Thyne et al., 2001). Therefore, in the TAGI sandstones, the observed change from dickitization to illitization may reflect an increase in burial temperature and/or the onset of oil emplacement. In the Middle–Upper TAGI reservoir, present-day temperature and fluid content (~110 °C, oil saturated) are consistent with a relatively recent timing for illitization.

5.2.2. Fe-dolomite cement

Fe-dolomite precipitated after minor compaction, as suggested by the kind of mutual contacts of some of the detrital grains enclosed within dolomite cement (Fig. 8a,b), but at relatively shallow depths (no more than a few hundred meters), as indicated by the high IGVs of the dolomite-cemented areas. Because the TAGI is overlain by up to ~150 m of Late Triassic and up to ~700 m of Liassic

deposits, dolomite precipitation most likely occurred during the latest Triassic or earliest Liassic.

The NE-trending field-bounding fault zone conditioned the distribution of dolomite cement. Dolomite is absent in well A, and is very rare in other wells of the ORD field (Chris Carr, pers. comm.). However, in well B, which is the only well located in the downthrown block of the fault, dolomite is common throughout the Middle–Upper TAGI. This fault belongs to a regional system of extensional faults whose movement is mainly latest Triassic in age (Cochran & Petersen, 2000). In the ORD field, this timing is supported by a significant thickness variation (~100 m) of the Late Triassic–earliest Liassic section across the fault zone. Because fault movement and dolomite cementation probably have similar timing, it is feasible that extensional faulting played a role in the distribution of dolomite cement, for instance by providing conduits for brine reflux.

The nature of the dolomite-precipitating waters cannot be established from the available data. However, taking into account the burial history and geological setting, it is likely that the dolomite precipitated from marine-derived waters. The TAGI is overlain by a ~850-m-thick Late Triassic–Liassic succession dominated by marginal marine evaporites. Large volumes of residual brine were undoubtedly generated during this prolonged period of evaporite deposition. Taking into account that such brines have a high potential for deep penetration via density-driven reflux (e.g. Stanislavsky & Gvirtzman, 1999), they most likely replaced the original connate waters of the TAGI during its shallow burial history. The precipitation of dolomite from such brines is favored because they normally have high salinities and high Mg/Ca ratios (Usdowski, 1994).

5.2.3. K-feldspar cement

K-feldspar overgrowths postdate dolomite cement but, similar to dolomite, they predate significant compaction and thus formed at relatively shallow burial depths, probably below a few hundred meters of overburden. K-feldspar precipitation requires high silica activities and high K^+/H^+ ratios (Morad et al., 2000). Refluxed residual brines associated with the Liassic halite evaporites are possible sources for K^+. It is unlikely, however, that the aluminum and silica necessary for K-feldspar precipitation were supplied by these brines, given the low concentrations of silica and aluminum in sea waters. Therefore, it is more likely that aluminum and silica were internally sourced by the alteration of detrital silicates, particularly feldspars. As discussed above, during shallow burial the TAGI sandstones were probably fluxed by hypersaline brines, which are normally acidic (Hanor, 1994) and thus capable of dissolving detrital feldspar. Other possible internal sources of silica, such as biogenic silica, pressure solution, or Illitization of smectitic clays, can be ruled out because: biogenic silica is absent, K-feldspar overgrowths predate pressure solution, and illitization of smectitic clays is temperature dependant and normally requires minimum burial depths of 1–2 km (Wood, 1994), inconsistent with the observation that K-feldspar overgrowths predate significant compaction.

Due to the greater chemical stability of authigenic with respect to detrital feldspar, it is feasible for feldspar overgrowths to have precipitated concurrently with the dissolution of detrital feldspars (De Ros, Sgarbi, & Morad, 1994). In the TAGI sandstones, the strong positive correlation between the contents in detrital and authigenic feldspar ($r^2 = 0.83$, $N = 30$) is consistent with this possibility, but such correlation may be also influenced by the higher availability of suitable nucleation surfaces in the sandstones richer in detrital feldspar.

5.2.4. Magnesite–siderite

Petrography shows that magnesite–siderite cement is multiphase and precipitated over a range of burial depths. The earliest generation (MS1), composed by ferroan magnesite, precipitated during relatively shallow burial, as indicated by the high IGV preserved within MS1 patches. Later generations, mainly composed by magnesian siderite, postdate compaction and thus precipitated during deeper burial.

The precipitation of diagenetic magnesite requires pore fluids with Mg/Ca molar ratios exceeding 40 (Aharon, 1988). Also, because aqueous Mg^{2+} is highly hydrated and thus relatively unreactive, the formation of magnesite at relatively low temperatures requires solutions of very high ionic strength, which are given by chloride solutions (Purvis, 1989; Usdowski, 1994). Magnesite precipitation is thus favored in halite-saturated evaporated sea waters, which are characterized by very high Mg/Ca molar ratios and high ionic strength (Usdowski, 1994). In the Berkine basin, such brines were certainly generated during the deposition of the Liassic evaporites, which include halite intervals exceeding 300 m in total thickness. Because the TAGI sandstones are located just below the evaporites, the residual brines should have migrated into them by means of density-driven reflux. Therefore, the magnesite cements probably precipitated during shallow burial from residual brines, related to the deposition of Liassic halite evaporites (cf. Garber, Harris, & Borer, 1990; Purvis, 1989). The precipitation of the TAGI magnesites from connate meteoric waters is unlikely, because these waters normally have low Mg/Ca ratios. Moreover, an enrichment in Mg of the initial meteoric waters is improbable because no Mg-rich rocks (such as ultramafic rocks or non-marine evaporites) are known in the area.

The high Fe^{2+} content of the MS1 magnesites indicates availability of reduced Fe^{2+}. Possible sources of Fe are the reduction of hematite and goethite, common in the Lower TAGI, or chlorite and biotite, present in minor amounts in the Middle–Upper TAGI. Later, burial-diagenetic more Fe-rich magnesite-siderite generations (MS2 and MS3) have compositions that indicate precipitation from waters with progressively higher Fe/Mg ratios.

5.2.5. Quartz cement

Quartz cement postdates significant compaction and has thus precipitated during relatively deep burial. It is likely that most of the silica required for quartz cementation was internally sourced by the pressure- or clay-induced dissolution of detrital quartz grains. This is suggested by the common presence of quartz dissolution features (intergranular dissolution contacts and stylolites) in most of the sandstones examined. Also, in the Lower TAGI, this source of silica for quartz cement is suggested by the alternation of: (1) relatively clay-poor sandstones rich in quartz cement, and (2) clay-coat-rich, more tightly compacted sandstones with little quartz cement and prominent quartz dissolution features.

As discussed above, in the Lower TAGI sandstones quartz cement is inhibited by grain-coating clay. This inhibition effect is commonly reported in the literature and is normally attributed to the reduction in surface area available for nucleation of authigenic quartz (e.g. Ehrenberg et al., 1993; Fisher, Knipe, & Worden, 2000). Grain-to-grain dissolution features are better developed in clay-coat-rich sandstones (Fig. 6A,C) than in nearby clay-coat-poor sandstones (Fig. 11A), indicating that intergranular illitic clays played a major role in quartz dissolution (cf. Bjørkum, 1996). It is thus reasonable to assume that clay-coat-rich sandstones exported silica to adjacent clay-coat-poor sandstones. In the Middle–Upper TAGI, there is no such alternation of clay-coat-poor and clay-coat-rich sandstones, but grain-to-grain dissolution features and stylolites are common.

Besides detrital quartz dissolution, clay–mineral reactions in intercalated mudstones might have contributed some additional silica for quartz cementation, especially in the Lower TAGI. This contribution would explain the anomalously high volumes of authigenic quartz observed in the clay-coat-poor sandstones from the uppermost part of the Lower TAGI, which occur intercalated between relatively thick mudstone intervals (Fig. 5).

Other possible additional source of silica for quartz cementation is the dissolution of K-feldspar during burial diagenesis, which releases silica and may result in the precipitation of quartz and illite (e.g. Barclay & Worden, 2000b; Bjørlykke & Egeberg, 1993). If kaolin is present in the system, the dissolution of K-feldspar may cause the illitization of kaolin, providing additional silica (Thyne et al., 2001). In the TAGI sandstones, petrography shows that a late-stage phase of dissolution indeed affects detrital and authigenic feldspar, and that some kaolin is illitized. Therefore, it is feasible that part of the silica required for quartz cementation is related with the late-stage dissolution of K-feldspar. However, because of the very low original feldspar content of the Lower TAGI sandstones, this potential source of silica could be significant only in the Middle–Upper TAGI. In any case, in this unit the average volume of feldspar-related secondary porosity is low (3.3%) compared to the average volume of authigenic quartz (9.2%), and thus the contribution of feldspar-sourced silica to quartz cement is probably subordinate.

At a local scale, the primary control on quartz cementation is the distribution of depositional clay, especially clay coatings. For this reason, the vertical distribution of quartz cement abundance cannot be used directly to evaluate the effect of oil charging on quartz cementation. It is known that oil charge can slow down quartz cementation and thus explain preferential quartz cementation in water zones (Marchand, Haszeldine, Macaulay, Swennen, & Fallick 2000; Worden & Barclay, 2000; Worden, Oxtoby, & Smalley, 1998). In fact, the second quartz generation is thicker in the samples located below a prominent bitumen-cemented interval located close to the present-day OWC and likely formed by means of selective removal of water-soluble compounds from the petroleum (cf. Barclay & Worden, 2000a).

5.2.6. Sulfate cements

Anhydrite and barite cements precipitated very late, because they postdate compaction and all the above-described authigenic phases. Both sulfates are usually found together in the same patches, suggesting that they are genetically related. The scarcity of quartz overgrowths inside some barite–anhydrite patches might indicate that some sulfate predated quartz overgrowth (cf. Morad et al., 1994). Nevertheless, anhydrite and barite usually replace previous phases, especially carbonates (Fig. 11G,H). As a consequence, the sulfates locally mimic the textural relationships of carbonate cements, which largely predate quartz cement. In conclusion, the scarcity of quartz overgrowths inside certain sulfate patches is compatible with the precipitation of all sulfate after quartz cementation, since the sulfates may have replaced pre-quartz carbonate cements.

The sulfate necessary for anhydrite and barite formation was likely sourced by the dissolution of anhydrite, which is abundant in the evaporite sequence overlying the TAGI. The deep subsurface dissolution of halite–anhydrite sequences normally produces sulfate-bearing brines (Hanor, 1994) from which anhydrite and barite cements may precipitate. Such a sulfate source has been demonstrated for numerous occurrences of late-stage barite and anhydrite cements in deeply buried sandstones from different basins (Dworkin & Land, 1994; Gluyas, Jolley, & Primmer, 1997; Greenwood & Habesch, 1997; Sullivan, Haszeldine, Boyce, Rogers, & Fallick, 1994).

Other possible sources for the sulfate of the TAGI anhydrites and barites appear unlikely. Sea water is not a likely source because: (1) sulfate concentrations in marine waters are rapidly depleted with depth (Dworkin & Land, 1994), and (2) the sulfates precipitated very late, when reflux of concentrated sea waters from the surface into the TAGI was improbable because of deep burial and sealing by a thick impervious evaporite section. The oxidation of pyrite is also an unlikely source of sulfate, because reducing conditions

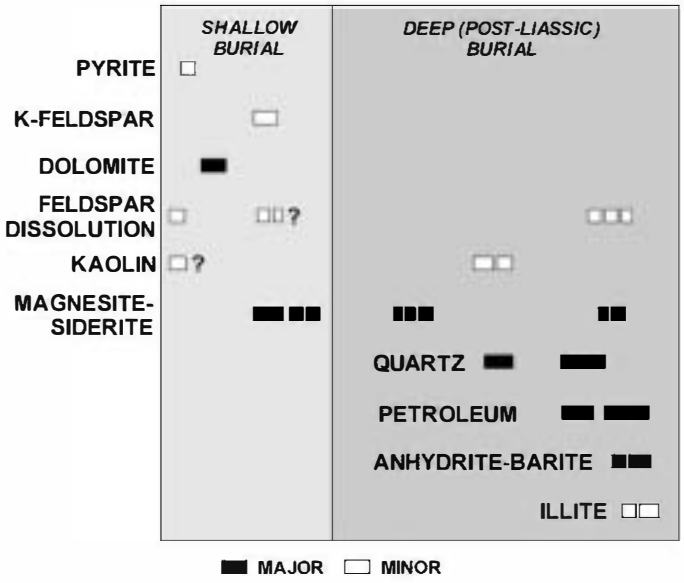

Fig. 14. Paragenetic sequence deduced from mutual textural relationships.

should normally prevail during the deep burial diagenesis of oil reservoir rocks.

The source of Ba^{2+} and Ca^{2+} for barite and anhydrite formation cannot be established from available data. However, an internal Ba^{2+} source is suggested by the stratigraphic distribution of barite cement, which is restricted to the Middle–Upper TAGI sandstones. A plausible internal Ba^{2+} source is the dissolution of detrital K-feldspar, since (1) detrital K-feldspars may contain barium, (2) petrography has shown that K-feldspar was partially dissolved during late-stage diagenesis, when barite cements formed, and (3) the Middle–Upper TAGI sandstones contain abundant detrital K-feldspar, which is virtually absent in the Lower TAGI. Similarly to barite, most anhydrite occurrences are restricted to the Middle–Upper TAGI, which would be consistent with a contribution of internally-sourced Ca^{2+}.

Because anhydrite and barite are probably late diagenetic and show no signs of dissolution, the sulfate-precipitating waters could have been relatively similar to the present-day formation brines. In the Triassic sandstone reservoirs of the central Berkine Basin, these brines are extremely saline (>350 g/l), Cl–Na–Ca–Mg dominated, but contain significant sulfate (Askri et al., 1995; Ben Dhia & Chiarelli, 1990; Morad et al., 1994; J. Navarro, pers. comm.). Although the origin of these brines is probably complex, their extremely high salinity suggest that the dissolution of evaporites might have played a role in their formation (cf. Hanor, 1994). Some compositional features of the present-day brines, such as the presence of sulfate, contents in Ca higher than in Mg, low Br concentrations, and low Br/Cl ratios, are also consistent with a significant contribution of solutes derived from the dissolution of halite–anhydrite evaporites (Carpenter, 1978; Hanor, 1994). Along the SE border of the Berkine Basin, gravity-driven flow of meteoric waters is currently taking place through TAGI-equivalent sandstones (Ben Dhia & Chiarelli, 1990; Boote et al., 1998; Chiarelli, 1978; Echikh, 1998). Salinity gradients and potentiometric data show that this flow does not currently affect the central part of the basin (Ben Dhia & Chiarelli, 1990). However, we cannot exclude this possibility during past humid climatic phases, providing thus a possible mechanism for deep subsurface dissolution of the Liassic evaporites.

Based on mutual textural relationships and the above discussion, the interpreted relative chronology of the different diagenetic features is summarized in Fig. 14.

5.3. *Implications for reservoir quality*

Provenance has influenced reservoir quality mainly by conditioning the distribution of detrital feldspars, which caused significant variation in the diagenetic paths followed by the Lower TAGI quartz arenites and the Middle–Upper TAGI subarkoses.

Secondary porosity created by the dissolution of feldspar is only significant in the Middle–Upper TAGI, where it has contributed notably (mean: 3.3%) to total porosity. However, this secondary porosity generation was balanced in part by the precipitation of by-products of feldspar dissolution, such as authigenic K-feldspar (mean: 1.3%) and kaolin (mean: 1.3%). Furthermore, the precipitation of sulfate cements is largely restricted to Middle–Upper TAGI sandstones (mean: 0.7%), possibly because feldspar dissolution provided the required cations.

The precipitation of late-diagenetic illite may critically influence the permeability of feldspar-bearing sandstones (e.g. Ramm and Ryseth, 1996; Midtbø et al., 2000). In the cored Middle–Upper TAGI section studied, however, illitization is incipient and thus seems not to be a critical factor for reservoir quality. This sandstone section is currently at

~3250 m of depth, where corrected present-day temperatures are ~110 °C (Yahi et al., 2001). Because illitization is influenced by temperature (Bjørlykke, 1998), the impact of late-diagenetic illite on permeability could be highly significant in more deeply buried Middle–Upper TAGI sandstone sections.

Other diagenetic factors, not directly controlled by detrital composition, have caused significant variation in reservoir quality within the TAGI. Compaction and especially quartz cementation are perhaps the most important. In the Lower TAGI, both factors are primarily controlled by the distribution of grain-coating clay, which is in turn facies controlled and thus potentially predictable. In the Lower TAGI, the content in grain-coating clay is stratigraphically variable, resulting in major variations of reservoir quality. Besides, quartz cement seems to be the main cause for the overall lower porosity of the Lower TAGI sandstones with respect to the Middle–Upper TAGI sandstones.

Cementation by dolomite accounts for a significant lateral variation in porosity. The areal distribution and paragenetic timing of the dolomite is consistent with the interpretation that cementation was favored in the downthrown block of the NE-trending, field-bounding fault. Porosity reduction by magnesite–siderite cement is of subordinate importance and has not produced any significant vertical variation in reservoir quality, at least in the studied sections. By contrast, some magnesite precipitated relatively early and thus may have acted as a framework-strengthening cement, inhibiting mechanical compaction, and thus contributing to porosity preservation.

6. Conclusions

1. There is a significant change in detrital composition between the Lower and Middle–Upper TAGI sandstones, caused by a change in provenance. The Lower TAGI quartz arenites were probably derived from Paleozoic siliciclastic rocks. By contrast, the Middle–Upper TAGI subarkoses most likely derive mainly from metamorphic terrains, presumably the Hoggar Massif, with a subordinate influence of granitic and sedimentary source areas. This change in provenance provides a potential criterion for stratigraphic correlation.
2. Grain-coating illitic and locally kaolinitic clays, common in the Lower TAGI sandstones, originated from pedogenesis and/or clay infiltration. Facies-related variations in the volume of grain-coating clay is one of the most important factors controlling the porosity and permeability of the Lower TAGI sandstones.
3. Shallow burial Fe-dolomite cementation occurred preferentially in the downthrown block of the NE-trending, field-bounding fault, causing significant lateral variations in porosity. Dolomite cementation was possibly related to the activity of this fault during the latest Triassic–earliest Liassic.
4. Magnesite–siderite cement is multiphase and precipitated over a range of burial depths. The earliest generation is composed by ferroan magnesite and precipitated during shallow burial from pore fluids with Mg/Ca molar ratios and very high ionic strength, possibly halite-saturated evaporated sea waters originated during the deposition of the Liassic evaporites and subsequently refluxed into the TAGI sandstones. Later magnesite–siderite generations precipitated during deeper burial from waters with progressively higher Fe/Mg ratios. Porosity reduction by magnesite–siderite cements has not produced any significant vertical variation in reservoir quality, at least in the studied sections.
5. K-feldspar overgrowths precipitated during shallow burial. Silica and aluminum were probably derived internally from the dissolution of detrital feldspar. Refluxed hypersaline brines possibly provided protons and high potassium activities, necessary for detrital feldspar dissolution and K-feldspar authigenesis, respectively.
6. The precipitation of authigenic vermicular kaolin was related to the dissolution of detrital feldspar. Kaolin largely consists of dickite, which replaced previously formed kaolinite. Dickitization occurred during relatively deep burial, and was postdated by a late-stage phase of illitization linked to the dissolution of detrital and authigenic K-feldspar. The change from dickitization to illitization may reflect increasing burial temperature and/or oil emplacement. Illitization is incipient and does not critically affect reservoir quality, at least in the cored section studied.
7. Quartz cement precipitated during deep burial. A significant part of the silica was internally sourced by the dissolution of detrital quartz. Feldspar-related reactions (in the Middle–Upper TAGI) and clay–mineral reactions in intercalated mudstones (in the Lower TAGI) might have contributed additional silica for quartz cementation.
8. Quartz cement is one of the most important factors controlling the reservoir quality of the TAGI sandstones. Quartz cement is the main cause of the lower average porosity of the Lower TAGI sandstones with respect to the Middle–Upper TAGI sandstones. The influence of quartz cement is particularly apparent within the Lower TAGI, where quartz cement abundance is stratigraphically very variable and results in prominent vertical variations in porosity and permeability. A large part of the variation in quartz cement is controlled by grain-coating clay, which in turn depends on depositional facies.
9. Anhydrite and barite cements precipitated very late. The sulfate necessary for their formation was likely sourced by the deep subsurface dissolution of the Late Triassic–Liassic evaporites overlying the TAGI. Cations were possibly derived internally from the dissolution of feldspars in the Middle–Upper TAGI.

10. Provenance has influenced the diagenesis mainly by conditioning the distribution of detrital feldspars. Feldspar-related secondary porosity, authigenic K-feldspar, vermicular kaolin, and sulfate cements are largely restricted to the Middle–Upper TAGI, but the influence on reservoir quality of these diagenetic products is probably higher for permeability than for porosity.

Acknowledgements

Cepsa and partners in the ORD field (Sonatrach, Anadarko Algeria Corp., Lasmo, Maersk, Burlington Resources, and Talisman) kindly provided permission to publish this work. Jorge Navarro and Chris Carr (Cepsa) are particularly thanked for their encouragement and discussions, and Terence Eschner (Sarlan Resources) is thanked for his useful comments on an early version of the manuscript. Alfredo Fernández-Larios is thanked for his assistance with the electron microprobe. Richard Worden and an anonymous reviewer are thanked for their careful reviews and critical comments.

References

Acheche, M. H., M'Rabet, A., Ghariani, H., Ouahchi, A., & Montgomery, S. L. (2001). Ghadames basin, southern Tunisia: a reappraisal of Triassic reservoirs and future prospectivity. *American Association of Petroleum Geologists Bulletin, 85*, 765–780.

Aharon, P. (1988). A stable-isotope study of magnesites from the Rum Jungle uranium field, Australia; implications for the origin of strata-bound massive magnesites. *Chemical Geology, 69*, 127–145.

Askri, H., Belmecheri, A., Benrabah, B., Boudjema, A., Boumendjel, K., Daoudi, M., Drid, M., Ghalem, T., Docca, A. M, Ghandriche, H., Ghomari, A., Guellati, N., Khemous, M., Lounici, R., Naili, H., Takherist, D., & Terkmani, D. (1995). Geology of Algeria. In M. S. Beghoul, A. Ghomari & M. Izem (Eds.), *Well Evaluation Conference Algeria 1995* (pp. I1–I93). Bath, UK: Schlumberger.

Barclay, S. A., & Worden, R. H. (2000a). Effects of reservoir wettability on quartz cementation in oil fields. In R. H. Worden & S. Morad (Eds.), *Quartz cement in sandstone reservoirs. Special Publication of the International Association of Sedimentologists, 29*, 103–117.

Barclay, S. A., & Worden, R. H. (2000b). Geochemical modeling of diagenetic reactions in a sub-arkosic sandstone. *Clay Minerals, 35*, 57–67.

Beard, D. C., & Weyl, P. K. (1973). Influence of texture on porosity and permeability of unconsolidated sand. In: *Diagenesis of Sandstones. American Association of Petroleum Geologists, Reprint series 20*, 349–369.

BenDhia, H., & Chiarelli, A. (1990). Hydrodynamic framework of Saharan Triassic aquifers in South Tunisia and Algeria. *Journal of African Earth Sciences, 10*, 585–589.

Ben Tahar, H. (1991). *Stratigraphy and sedimentology of Triassic sandstones, El Borma oil field and southern Tunisia*. PhD dissertation, Colorado State University, 184 pp.

Bjørkum, P. A. (1996). How important is pressure in causing dissolution of quartz in sandstones? *Journal of Sedimentary Research, 66*, 147–154.

Bjørlykke, K. (1998). Clay mineral diagenesis in sedimentary basins: a key to the prediction of rock properties. Examples from the North Sea Basin. *Clay Minerals, 33*, 15–34.

Bjørlykke, K., & Egeberg, P. K. (1993). Quartz cementation in sedimentary basins. *American Association of Petroleum Geologists Bulletin, 77*, 1538–1548.

Bloch, S. (1994). Effect of Detrital Mineral Composition on Reservoir Quality. In M. D. Wilson (Ed.), *Reservoir Quality Assessment and Prediction in Clastic Rocks. Society of Economic Paleontologists and Mineralogists Short Course, 30*, 161–182.

Boote, R. D., Clark-Lowes, D. D., & Traut, M. W. (1998). Paleozoic petroleum systems of North Africa. In D. S. MacGregor, R. T. J. Moody & D. D. Clark-Lowes (Eds.), *Petroleum geology of North Africa. Geological Society of London Special Publication, 132*, 7–68.

Boudjema, A. (1987). *Evolution structural du bassin pétrolier—Triassique—du Sahara Nord Oriental (Algérie)*. These l'Université de Paris-Sud, Centre d'Orsay, Paris, Editions Technip, 279 pp.

Carney, S. R., Peffer, J. W., Pink, A., Drumheller, R. E., Jasek, J. H., Hadjali, M., & Bouazza, L. (1999). The Hassi Berkine South (HBNS) Field, Block 404, Berkine Basin, Algeria. *American Association of Petroleum Geologists, Annual Meeting*, Expanded Abstracts, San Antonio, Texas, United States, p. A21.

Carpenter, A. B. (1978). Origin and chemical evolution of brines in sedimentary basins. *Oklahoma Geological Survey Circular, 79*, 78–88.

Chiarelli, A. (1978). Hydrodynamic framework of eastern Algerian Sahara—influence on hydrocarbon occurrence. *American Association of Petroleum Geologists Bulletin, 62*, 667–685.

Cochran, M. D., & Petersen, L. E. (2000). Hydrocarbon exploration in the Berkine Basin, Grand Erg Oriental, Algeria. Second Wallace E. Pratt Memorial Conference on Petroleum Provinces of the 21st Century, San Diego, California, January 12–15, 2000. *American Association of Petroleum Geologists*, 28 pp.

Daniels, R. P, Hook, R. C., Sorensen, P. R., & Emme, J. J. (1994). Triassic depositional system and reservoir development, Ghadames Basin, Algeria. *American Association of Petroleum Geologists.* Annual Convention, Annual Meeting Abstracts, p. 131.

De Ros, L. F., Sgarbi, G. N. C., & Morad, S. (1994). Multiple authigenesis of K-feldspar in sandstones; evidence from the Cretaceous Areado Formation, Sao Francisco Basin, central Brazil. *Journal of Sedimentary Research, 64*, 778–787.

Dickinson, W. R. (1985). Interpreting provenance relations from detrital modes of sandstones. In G. G. Zuffa (Ed.), *Provenance of arenites. NATO ASI Series, vol. 148* (pp. 333–361). Dordrecht: Reidel.

Dworkin, S. I., & Land, L. S. (1994). Petrographic and geochemical constraints on the formation and diagenesis of anhydrite cements, Smackover sandstones, Gulf of Mexico. *Journal of Sedimentary Research, A64*, 339–348.

Echikh, K. (1998). Geology and hydrocarbon occurrences in the Ghadames Basin, Algeria, Tunisia, Libya. In D. S. MacGregor, R. T. J. Moody & D. D. Clark-Lowes (Eds.), *Petroleum geology of North Africa. Geological Society of London Special Publication, 132*, 109–130.

Ehrenberg, S. N., Aagaard, P., Willson, M. J., Fraser, A. R., & Duthie, D. M. L. (1993). Depth-dependent transformation of kaolinite to dickite in sandstones of the Norwegian continental shelf. *Clay Minerals, 28*, 325–352.

Fisher, Q. J., Knipe, R. J., & Worden, R. H. (2000). Microstuctures of deformed and non-deformed sandstones from the North Sea: Implications for the origins of quartz cement in sandstones. In R. H. Worden & S. Morad (Eds.), *Quartz cement in sandstone reservoirs. Special Publication of International Association of Sedimentologists, 29*, 129–146.

Ford, G. W., & Scott, A. J. (1997). A depositional model and sequence stratigraphy of the Trias Argilo-Greseux Inferieur (T.A.G.I.) in the Ghadames Basin, Algeria. *American Association of Petroleum Geologists, 1997 Annual Convention Abstracts*, p. 36.

Garber, R. A., Harris, P. M., & Borer, J. M. (1990). Occurrence and significance of magnesite in Upper Permian (Guadalupian) Tansill and Yates Formations, Delaware Basin, New Mexico. *American Association of Petroleum Geologists Bulletin, 74*, 119–134.

Gauthier, F. J., Boudjema, A., & Lounis, R. (1995). The structural evolution off the Ghadames and Illizi basins during the Paleozoic, Mesozoic, and Cenozoic; petroleum implications. AAPG International Conference and Exhibition, Abstracts. *American Association of Petroleum Geologists Bulletin, 79*, 1214–1215.

Gluyas, J., & Cade, C. A. (1997). Prediction of porosity in compacted sands. In J. A. Kupecz, J. Gluyas & S. Bloch (Eds.), *Reservoir quality*

prediction in sandstones and carbonates. American Association of Petroleum Geologists Memoir, 69, 19–28.

Gluyas, J., Jolley, L., & Primmer, T. J. (1997). Element mobility during diagenesis; sulfate cementation of Rotliegend sandstones, southern North Sea. *Marine Petroleum Geology, 14*, 1001–1011.

Greenwood, P. J., & Habesch, S. M. (1997). Diagenesis of the Sherwood Sandstone Group in the southern East Irish Sea basin (blocks 110/13, 110/14 and 110/15); constraints from preliminary isotopic and fluid inclusion studies. In N. S. Meadows, S. P. Trueblood, M. Hardman & G. Cowan (Eds.), *Petroleum geology of the Irish Sea and adjacent areas. Geological Society of London Special Publication, 124*, 353–371.

Hanor, J. S. (1994). Origin of saline fluids in sedimentary basins. In J. Parnell (Ed.), *Geofluids: Origin, migration and evolution of fluids in sedimentary basins. Geological Society of London Special Publication, 78*, 151–174.

Jackson, J. S., Moore, S. R., Quarles, A. I., & Bellis, J. (1996). Post-Paleozoic deformation in the Triassic Basin, North Africa. *American Association of Petroleum Geologists, Annual Convention*, San Diego, United States, Abstracts, p. 70.

Lundegard, P. D. (1992). Sandstone porosity loss—a 'big picture' view of the importance of compaction. *Journal of Sedimentary Petrology, 62*, 250–260.

MacGregor, D. S. (1998a). Introduction. In D. S. MacGregor, R. T. J. Moody & D. D. Clark-Lowes (Eds.), *Petroleum geology of North Africa. Geological Society of London Special Publication, 132*, 1–6.

MacGregor, D. S. (1998b). Giant fields, petroleum systems and exploration maturity of Algeria. In D. S. MacGregor, R. T. J. Moody & D. D. Clark-Lowes (Eds.), *Petroleum geology of North Africa. Geological Society of London Special Publication, 132*, 79–96.

Makhous, M., Galushkin, Y., & Lopatin, N. (1997). Burial history and kinetic modeling for hydrocarbon generation, Part II: Applying the GALO model to Saharan basins. *American Association of Petroleum Geologists Bulletin, 81*, 1679–1699.

Marchand, A. M. E., Haszeldine, R. S., Macaulay, C. I., Swennen, R., & Fallick, A. E. (2000). Quartz cementation inhibited by crestal oil charge; Miller deep water sandstone, UK North Sea. *Clay Minerals, 35*, 201–210.

Matter, A., & Ramseyer, K. (1985). Cathodoluminescence microscopy as a tool for provenance study of sandstones. In G. G. Zuffa (Ed.), *Provenance of arenites. NATO ASI series, vol. 148* (pp. 191–211). Dordrecht: Reidel.

Midtbø, R. E. A., Rykkje, J. M., & Ramm, M. (2000). Deep burial diagnesis and reservoir quality along the eastern flank of Viking Graben; evidence for illitization and quartz cementation after hydrocarbon emplacement *Clay Minerals, 35*, 227–237.

Morad, S., Ben Ismail, H., De Ros, L. F., Al-Aasm, I. S., & Serrhini, N. E. (1994). Diagenesis and formation waters chemistry of Triassic reservoir sandstones from southern-Tunisia. *Sedimentology, 41*, 1253–1272.

Morad, S., Ketzer, J. M., & De Ros, F. (2000). Spatial and temporal distribution of diagenetic alterations in siliciclastic rocks: Implications for mass transfer in sedimentary basins. *Sedimentology, 47*, 95–120.

Moraes, M. A. S., & De Ros, L. F. (1990). Infiltrated clays in fluvial Jurassic sandstones of Reconcavo Basin, northeastern Brazil. *Journal of Sedimentary Petrology, 60*, 809–819.

Morton, A., & Hurst, A. (1995). Correlation of sandstones using heavy minerals: An example from the Statfjord Formation in the Snorre Field, northern North Sea. In R. E. Dunay & E. A. Hailwood (Eds.), *Non-biostratigraphical methods of dating and correlation. Geological Society of London Special Publication, 89*, 3–22.

Owen, M. R. (1991). Application of cathodoluminescence to sandstone provenance. In C. E. Barker & O. C. Kopp (Eds.), *Luminescence microscopy: Quantitative and qualitative aspects. Society of Economic Paleontologists and Mineralogists Short Course, 25*, 67–75.

Pittman, E. D. (1992). Artifact porosity in thin sections of sandstones. *Journal of Sedimentary Petrology, 62*, 734–737.

Pittman, E. D., Larese, R. E., & Meald, M. T. (1992). Clay coats: Occurrence and relevance to preservation of porosity. In D. W. Houseknecht & E. D. Pittman (Eds.), *Origin, diagenesis, and petrophysics of clay minerals in sandstones. Society of Economic Paleontologists and Mineralogists Special Publication, 47*, 241–255.

Purvis, K. (1989). Zoned authigenic magnesites in the Rotliegend Lower Permian, southern North Sea. *Sedimentary Geology, 65*, 307–318.

Ramm, M., & Ryseth, A. E. (1996). Reservoir quality and burial diagenesis in the Statfjord Formation, North Sea. *Petroleum Geoscience 2*, 313–324.

Scott, A. J., & Howells, C. (2000). Analogues for the Trias Argil-Gréseux Inferieur (TAGI), Berkine Basin, Algeria. *Turning the Conventional into the Unconventional, an Integrated Approach.* Sonatrach JST-4 Conference, April 2000, Algiers, Algeria.

Scott, A. J., & Wheller, D. A. (1999). Regional trends in Triassic fluvial–lacustrine cycles, Berkine Basin, Algeria. *American Association of Petroleum Geologists Annual Meeting Expanded Abstracts*, San Antonio, Texas, United States, p. A126.

Shirley, K. (2000). Big implications for supply needs—discoveries are getting smaller. *American Association of Petroleum Geologists Explorer, January*, 6–14.

Stanislavsky, E., & Gvirtzman, H. (1999). Basin-scale migration of continental-rift brines: Paleohydrologic modeling of the Dead Sea basin. *Geology, 27*, 791–794.

Sullivan, M. D., Haszeldine, R. S., Boyce, A. J., Rogers, G., & Fallick, A. E. (1994). Late anhydrite cements mark basin inversion; isotopic and formation water evidence, Rotliegend Sandstone, North Sea. *Marine Petroleum Geology, 11*, 46–54.

Thyne, G., Boudreau, B. P., Ramm, M., & Midtbø, R. E. (2001). Simulation of potassium feldspar dissolution and illitization in the Statfjord Formation, North Sea. *American Association of Petroleum Geologists Bulletin, 85*, 621–637.

Turner, P., Pilling, D., Walker, D., Exton, J., Binnie, J., & Sabaou, N. (2001). Sequence stratigraphy and sedimentology of the late Triassic TAGI-I (Blocks 401–402, Berkine Basins, Algeria). *Marine Petroleum Geology, 18*, 959–981.

Usdowski, E. (1994). Synthesis of dolomite and geochemical implications. In B. Purser, M. Tucker & D. Zenger (Eds.), *Dolomites. Special Publication of the International Association of Sedimentologists, 21*, 345–360.

Walker, T. R., Waugh, B., & Crone, A. J. (1978). Diagenesis in first cycle desert alluvium of Cenozoic age, southwestern United States and northwestern Mexico. *Geological Society of America Bulletin, 89*, 19–32.

Wheller, D. A., Carney, S. R., Drumheller, R. E., Winstanley, S. I., Hadjali, M., & Scott, A. J. (1999). Sedimentology and reservoir characterization of the Hassi Berkine South (HBNS) Field, Block 404, Berkine Basin, Algeria. American Association of Petroleum Geologists International Conference and Exhibition, Birmingham, United Kingdom. *American Association of Petroleum Geologists Bulletin, 83*, p. 1345.

Wilson, M. D., & Stanton, P. T. (1994). Diagenetic mechanisms of porosity and permeability reduction and enhancement. In M. D. Wilson (Ed.), *Reservoir quality assessment and prediction in clastic rocks. Society of Economic Paleontologists and Mineralogists Short Course, 30*, 59–118.

Wood, J. R. (1994). Chemical diagenesis. In M. D. Wilson (Ed.), *Reservoir quality assessment and prediction in clastic rocks. Society of Economic Paleontologists and Mineralogists Short Course, 30*, 119–136.

Worden, R. H., & Barclay, S. A. (2000). Internally-sourced quartz cement due to externally-derived CO_2 in sub-arkosic sandstones, North Sea. *Journal of Geochemical Exploration, 69–70*, 645–649.

Worden, R. H., Oxtoby, N. H., & Smalley, P. C. (1998). Can oil emplacement prevent quartz cementation in sandstones? *Petroleum Geoscience, 4*, 129–137.

Yahi, N., Schaefer, R. G., & Littke, R. (2001). Petroleum generation and accumulation in the Berkine basin, eastern Algeria. *American Association of Petroleum Geologists Bulletin, 85*, 1439–1467.